

Aus dem Friedrich-Baur-Institut
an der Neurologischen Klinik und Poliklinik
Klinik der Universität München
Direktor: Prof. Dr. Günter Höglinger

Characterization of novel *TOR1A* variants causing
extreme phenotypes of arthrogryposis multiplex con-
genita

Dissertation
zum Erwerb des Doktorgrades der Medizin
an der Medizinischen Fakultät der
Ludwig-Maximilians-Universität zu München

vorgelegt von
Michael Thomas Pascher
aus
Filderstadt
2023

Mit Genehmigung der Medizinischen Fakultät
der Universität München

Berichterstatter: Prof. Dr. Jan Senderek

Mitberichterstatter: Prof. Dr. Florian Heinen
PD Dr. Beate Häberle

Mitbetreuung durch die
promovierte Mitarbeiterin: Dr. Marina Dusl

Dekan: Prof. Dr. Thomas Gudermann

Tag der mündlichen Prüfung: 13.07.2023

Table of contents

Table of contents	3
Acknowledgements	5
List of figures	6
List of tables	6
Abbreviations	8
1 Summary	11
2 Zusammenfassung	12
3 Introduction	14
3.1 Primary early-onset torsion dystonia (DYT1).....	14
3.2 <i>TOR1A</i> related arthrogryposis multiplex congenita	14
3.3 TorsinA – an AAA+ ATPase	15
3.4 Current understanding of torsinA’s cellular function.....	16
3.4.1 TorsinA as a regulator of LINC complex assembly	16
3.4.2 TorsinA-dependent LINC complex formation and cell migration	16
3.4.3 TorsinA in nuclear envelope morphology and nucleo-cytosolic transport	17
3.4.4 Other possible roles for torsinA in cell function	17
4 Material and methods	19
4.1 Materials	19
4.1.1 Laboratory equipment	19
4.1.2 Chemicals	20
4.1.3 Molecular biology kits and enzymes	20
4.1.4 Oligonucleotides.....	22
4.1.5 Plasmids.....	23
4.1.6 Antibodies.....	25
4.1.7 <i>E. coli</i> strains	26
4.1.8 Mammalian cell lines	26
4.2 Methods	27
4.2.1 <i>In silico</i> prediction tools	27
4.2.2 Microbiological methods.....	27
4.2.3 Nucleic acid methods	29
4.2.4 Mammalian cell culture.....	35
4.2.5 Protein methods	37
4.2.6 Immunofluorescence microscopy.....	38
4.2.7 Dual luciferase reporter assay	38
4.2.8 Statistical analysis	39

5	Results	40
5.1	Identification of <i>TORIA</i> variants in AMC patients.....	40
5.2	Sanger sequencing of patients with similar phenotypes.....	40
5.3	<i>In silico</i> assessment of pathogenicity of identified variants.....	42
5.4	Clinical presentation of <i>TORIA</i> related AMC.....	44
5.5	Levels of overexpressed wild-type and mutant torsinA in HEK293 cells.....	48
5.6	Degradation kinetics of wild-type and mutant torsinA.....	49
5.7	Degradation of wild-type and mutant torsinA through proteasome and autophagy pathways.....	50
5.8	Effect of <i>TORIA</i> variants on torsinA's subcellular localization.....	52
5.9	TorsinA levels associated with the <i>TORIA</i> c.-3G>T variant.....	53
5.10	Translational activity of the <i>TORIA</i> c.-3G>T cDNA.....	54
5.11	Effect of <i>TORIA</i> variants on LAP1 and LULL1 localization.....	55
5.12	Effects of <i>TORIA</i> variants on nuclear movement in polarizing cells.....	57
5.13	Effects of <i>TORIA</i> variants on fibroblast migration.....	58
6	Discussion	61
7	Supplemental material	65
7.1	Whole exome sequencing output.....	65
7.2	<i>In silico</i> analysis results.....	66
7.3	Detailed information about clinical findings of <i>TORIA</i> -related AMC cases.....	68
7.3.1	General information, pregnancy and birth history.....	68
7.3.2	Disease course.....	69
7.3.3	Further diagnostic studies.....	70
7.4	Anti-TorsinA (D-M2A8) antibody.....	70
7.5	TorsinA expression in fibroblasts of AMC-cases.....	71
7.6	Relative <i>TORIA</i> mRNA levels in fibroblasts of AMC cases.....	72
7.7	Online tools.....	72
7.7.1	<i>In silico</i> prediction tools.....	72
7.7.2	Genome and exome databases.....	72
7.7.3	Tools for primer design and cloning.....	73
7.7.4	Other online tools.....	73
8	Contributions	74
9	References	75
10	Eidesstattliche Versicherung	83

Acknowledgements

I want to thank Prof. Dr. med. Marianne Dieterich for giving me the opportunity of doing my thesis at the Friedrich-Baur-Institute in the laboratory of molecular myology in a very helpful and professional team.

Dear Jan, I really want to thank you for proposing the topic of my thesis and your support before, during and after my time in the laboratory. I have very much appreciated having such a competent physician and scientist on my side helping me out at critical phases of my study.

A very special thank-you to you, Marina, for teaching me all the laboratory technics, for supporting me in presentations and scientific reports and always being a helping hand. I really appreciated working with you during my time in the lab! I had a great time! Thank you so much!

Furthermore, I want to thank you, Stefan, for being practical and mental support during good and hard times. I will miss our time together in the lab and outside on the ski slopes or in Erding!

Thank you, Rolf, for always lending a sympathetic ear for all my problems and helping me out in difficult situations. I appreciated your experience, knowledge and resourcefulness.

And I want to thank Peter and Sarah for the fun time we had together! I will never forget sharing French fries with Lenia and never forget joking in the lab with you, Peter!

Dear Lisa, thank you for your support and the fun hours we spend together in cell culture and outside the lab! You made my time in the lab a very pleasant one. I'm very grateful for meeting you there and finally having you by my side!

Finally, a special thank you to my parents, my sister and my grandparents. Thank you for supporting me throughout my studies and this thesis. Without your help, this would have been impossible. Thank you so much.

List of figures

Figure 1: DYT1- and AMC-related variants in <i>TOR1A</i>	41
Figure 2: <i>TOR1A</i> variants identified in families A and C.....	41
Figure 3: Primary and tertiary structures of torsinA.....	43
Figure 4: Multiple Sequence Alignments (MSA) for p.Ser112Arg and c.-3G>T variants.....	44
Figure 5: Pedigrees of families A, B and C.....	46
Figure 6: Clinical photographs of individuals with biallelic <i>TOR1A</i> variants.....	47
Figure 7: Levels of p.Ser112Arg and p.Arg288* torsinA-GFP in HEK293 cells....	48
Figure 8: Cycloheximide chase followed by western blotting.....	50
Figure 9: Effect of proteasome inhibition on torsinA-GFP levels.....	51
Figure 10: Effect of autophagy inhibition on torsinA-GFP levels.....	52
Figure 11: Immunofluorescence staining of HeLa cells transiently transfected with <i>TOR1A</i> -GFP constructs.....	53
Figure 12: Western blot analysis of the c.-3G>T <i>TOR1A</i> variant.....	54
Figure 13: Dual luciferase reporter assay of the c.-3G>T variant.....	55
Figure 14: Immunofluorescence staining of primary skin fibroblasts transiently transfected with LAP1- and LULL1-HA constructs.....	57
Figure 15: Centrosome reorientation in polarizing patient and control fibroblasts.....	58
Figure 16: Wound healing assay using patients' dermal fibroblasts.....	59
<u>Supplemental figures:</u>	
Figure S1: Anti-torsinA (D-M2A8) antibody.....	70
Figure S2: Endogenous torsinA levels in dermal fibroblasts of AMC-cases.....	71
Figure S3: Relative <i>TOR1A</i> mRNA levels in dermal fibroblasts of AMC cases.....	72

List of tables

Table 1: Oligonucleotides for detection of <i>TOR1A</i> variants.....	22
Table 2: Oligonucleotides for cDNA amplification.....	22
Table 3: Oligonucleotides for site-directed mutagenesis.....	22
Table 4: Oligonucleotides for qRT-PCR.....	23
Table 5: Oligonucleotides for plasmid sequencing.....	23
Table 6: Overview of plasmids used in this study.....	23
Table 7: Primary antibodies.....	25
Table 8: Secondary antibodies.....	26
Table 9: <i>E. coli</i> strains.....	26
Table 10: Reaction mix for colony PCR.....	30
Table 11: PCR program for colony PCR.....	31
Table 12: Reaction mix for amplification of genomic DNA.....	31

Table 13: PCR program for exon amplification of genomic DNA	31
Table 14: Reaction mix for real-time qRT-PCR	33
Table 15: PCR program for real-time qRT-PCR	33
Table 16: Restriction digest reaction mix for testing plasmid identity	34
Table 17: Restriction digest reaction mix for plasmid generation	34
Table 18: Reaction mix for ligation	34
Table 19: Sample preparation for SDS-PAGE	37
Table 20: <i>TOR1A</i> variants and their frequencies in global databases	41
<u>Supplemental tables:</u>	
Table S1: Whole exome sequencing output	65
Table S2: In silico analysis results (continued on following page)	66
Table S3: General information, pregnancy and birth history	68
Table S4: Disease course	69
Table S5: Further diagnostic studies	70

Abbreviations

aa	amino acid
AMC	arthrogryposis multiplex congenita
bp	base pair/s
BSA	bovine serum albumin
°C	degree Celsius
cDNA	complementary DNA
CK	creatine kinase
CNS	central nervous system
CS	coverslip/s
CT	computed tomography
d	day/s
ddH ₂ O	double-distilled water
DMSO	dimethyl sulfoxide
DNA	deoxyribonucleic acid
DYT1	early-onset torsion dystonia/primäre Torsionsdystonie Typ 1
<i>E. coli</i>	<i>Escherichia coli</i>
EDTA	ethylenediaminetetraacetic acid
EEG	electroencephalography
e.g.	exempli gratia, for example
EMG	electromyography
ER	endoplasmic reticulum
et al.	et alia, and others
FCS	fetal calf serum
g	gram
GAPDH	glyceraldehyde 3-phosphate dehydrogenase
GFP	green fluorescent protein
h	hour/hours
HEK293	human embryonic kidney 293
HeLa	Henrietta Lacks
HS	horse serum

IF	immunofluorescence
l	liter
kb	kilobase
kDa	kilodalton
LB	Luria-Bertani
LINC	linker of nucleoskeleton and cytoskeleton
M	molar
m	mass
MCS	multiple cloning site
min	minutes
ml	milliliter
mM	millimolar
MOPS	3-(N-morpholino)propanesulfonic acid
MRI	magnetic resonance imaging
mRNA	messenger ribonucleic acid
MSA	multiple sequence alignment
mut	mutant
NE	nuclear envelope
ng	nanogram
nm	nanometer
o.n.	over night
ORF	open reading frame
PBS	phosphate buffered saline
PCR	polymerase chain reaction
qRT-PCR	quantitative reverse transcription PCR
RNA	ribonucleic acid
rpm	revolutions per minute
rt	room temperature
RT	reverse transcription
SDS	sodium dodecyl sulfate
sec	second/s
SNP	single nucleotide polymorphism

Tris	Tris-(hydroxymethyl)-aminomethane
U	unit/s
UTR	untranslated region
UV	ultraviolet
wt	wild type
WB	western blot
μg	microgram
μl	microliter
μm	micrometer

1 Summary

The *TOR1A* gene encodes torsinA, an AAA+ ATPase that exerts multiple functions, including nuclear envelope homeostasis and regulation of centrosome orientation and cell migration. A single amino acid deletion (p.Glu303del) in torsinA causes a long-recognized low-penetrance autosomal dominant disorder, torsion dystonia-1. More recently, biallelic *TOR1A* variants have been linked to an additional condition, an autosomal recessive congenital arthrogryposis syndrome complicated by global developmental delay.

This study extends the clinical and mutation spectrum of the *TOR1A*-associated contracture syndrome: Four patients carried a homozygous variant c.862C>T (p.Arg288*) and presented with severe contractures, massive global developmental delays, generalized muscle weakness, bulbar dysfunction and respiratory failure. All four infants died within the first 11 weeks of life. One case with compound heterozygous variants c.-3G>T and c.336C>A (p.Ser112Arg) presented with a much milder phenotype consisting of congenital contractures, motor delay, spastic paraparesis and moderate cognitive deficits. Contractures largely improved over time and were only slightly debilitating when last examined at age eight years.

Arthrogryposis-related *TOR1A* variants led to decreased cellular levels of torsinA. Low levels of the p.Ser112Arg and p.Arg288* variants seem to result from increased protein turnover by the proteasome. Conversely, the 5'-UTR variant c.-3G>T, affecting a highly conserved base in the *TOR1A* Kozak sequence, appears to affect protein levels by impairing translation efficiency. The p.Ser112Arg variant also altered torsinA subcellular localization, which may further reduce availability of torsinA at its site of physiological action. In patient-derived dermal fibroblasts, strong reduction of torsinA levels (homozygous p.Arg288*) impaired positioning of centrosomes and cell motility, consistent with disruption of known torsinA functions.

In conclusion, biallelic *TOR1A* mutations alter properties of torsinA and its cellular functions and cause variable forms of arthrogryposis. Pathogenicity of *TOR1A* variants was supported by altered properties of mutant torsinA and torsinA-deficient patient-derived cells, even though it is still unclear how disruption of torsinA functions eventually leads to disease.

2 Zusammenfassung

TorsinA ist eine AAA⁺-ATPase, welche durch das Gen *TOR1A* kodiert wird. TorsinA erfüllt eine Vielzahl zellulärer Funktionen, unter anderem spielt es bei der Aufrechterhaltung der Struktur der Kernhülle, der Positionierung der Zentrosomen und der Zellmigration eine wichtige Rolle. Die Deletion einer einzelnen Aminosäure (p.Glu303del) in TorsinA verursacht eine lang bekannte unvollständig penetrante autosomal-dominante Erkrankung, die Torsionsdystonie Typ 1. Kürzlich wurden bi-allelische *TOR1A*-Varianten mit einer weiteren Erkrankung in Verbindung gebracht, einem angeborenen autosomal-rezessiv vererbten Arthrogrypose-Syndrom, dessen Klinik zusätzlich durch eine globale Entwicklungsverzögerung geprägt ist.

Diese Studie erweitert das Spektrum der Mutationen und Klinik *TOR1A*-assoziierter Arthrogryposen: Vier Patienten trugen eine homozygote Variante c.862C>T (p.Arg288*) und zeigten ausgeprägte Kontrakturen, massive globalen Entwicklungsverzögerung, generalisierte Muskelschwäche, bulbäre Funktionsstörungen und respiratorische Insuffizienz. Alle vier Säuglinge starben innerhalb der ersten 11 Lebenswochen. Ein Patient mit den „compound heterozygoten“ Varianten c.-3G>T und c.336C>A (p.Ser112Arg) zeigte einen viel milderen Phänotyp aus angeborenen Kontrakturen, motorischer Entwicklungsverzögerung, spastischer Paraparese und moderaten kognitiven Defiziten. Die Kontrakturen besserten sich im Laufe der Zeit weitgehend und führten bei der letzten Untersuchung im Alter von acht Jahren nur noch zu leichten körperlichen Einschränkungen.

Die Arthrogrypose-assoziierten *TOR1A*-Varianten gingen mit reduzierten zellulären TorsinA-Spiegeln einher. Diese niedrigen Konzentrationen der p.Ser112Arg- und p.Arg288*-Varianten scheinen durch einen beschleunigten proteasomalen Proteinumsatz bedingt zu sein. Im Gegensatz dazu scheint die 5'-UTR-Variante c.-3G>T, die eine hochkonservierte Base in der *TOR1A*-Kozak-Sequenz betrifft, die Proteinspiegel durch Beeinträchtigung der Translationseffizienz zu vermindern. Die p.Ser112Arg-Variante veränderte zudem die subzelluläre Lokalisation von TorsinA, was die Verfügbarkeit von TorsinA am Ort seiner physiologischen Aktivität weiter verringern könnte. In Hautfibroblasten der Patienten beeinträchtigte eine starke Verringerung der TorsinA-Spiegel (homozygote variante p.Arg288*) die Positionierung von Zentrosomen und die Zellmotilität, was mit einer Störung bekannter TorsinA-Funktionen in Einklang steht.

Zusammenfassend kann festgehalten werden, dass biallelische *TOR1A*-Mutationen die Eigenschaften von TorsinA und seine Zellfunktionen verändern und verschiedene

Ausprägungen angeborener Arthrogryposen verursachen können. Die Pathogenität von *TORIA*-Varianten wurde durch den Nachweis veränderter Eigenschaften von mutiertem TorsinA und TorsinA-defizienten Patientenzellen untermauert, wenngleich noch unklar ist, wie eine Störung von TorsinA-Funktionen letztendlich zum Auftreten der Erkrankung führt.

3 Introduction

3.1 Primary early-onset torsion dystonia (DYT1)

Dystonia was first described by Oppenheim as “dystonia musculorum deformans“ about 100 years ago [1]. Dystonias are a group of neurological disorders defined by involuntary, persistent muscle contractions resulting in repetitive and twisting movements and abnormal postures [2]. An important step in clarifying the pathogenesis of dystonias was the discovery that a heterozygous three base pair (GAG) deletion in the *TOR1A* gene and subsequent loss of a glutamic acid (p.Glu303del) in the torsinA protein cause primary early-onset torsion dystonia (DYT1) [3]. Inheritance was found to be autosomal dominant with incomplete penetrance of about 30-40 % [4]. Exact figures for prevalence do not exist, but a recent study estimated the prevalence in the USA to 5.3-7.9:100,000 [5]. Clinically, DYT1 is characterized by early onset of symptoms, starting in a single limb, spreading to other body parts and later generalization with cranial and cervical regions usually spared [6, 7]. Except for tremor, no other neurological deficits accompany these symptoms [8]. Brain computed tomography (CT) or magnetic resonance imaging (MRI) scans are typically unremarkable [9]. Post mortem examination of brains of affected individuals is generally normal. One study described perinuclear inclusions in brainstem neurons [10]; however, this finding was not replicated in later studies [11].

There is still no causal therapy for DYT1 dystonia. Treatment is limited to symptomatic therapy including oral medication with anticholinergics and local botulinum toxin injections [12, 13]. In case of therapy refractory symptoms, deep brain stimulation can be considered [14].

In addition to the common GAG deletion, several additional *TOR1A* variants have been identified in patients with dystonia in the last two decades [15-21]; however, pathogenicity of most of these variants has remained unclear [20, 22].

3.2 *TOR1A* related arthrogyriposis multiplex congenita

Arthrogyriposis multiplex congenita (AMC) is a heterogeneous condition defined by multiple joint contractures that affect at least two body areas present at birth [23, 24]. Its prevalence is estimated between 1:3,000 and 1:5,000 [25]. The etiology of this condition is broad and includes maternal causes, complications during pregnancy and fetal abnormalities such as muscular, neurological or connective tissue disorders [24, 26]. The

severity of contractures, the number of affected joints and additional organ involvements vary dependent on the primary cause of AMC [23]. Spreading of contractures to initially unaffected joints is uncommon [23].

In 2017, Kariminejad et al. published a series of four children with AMC, either homozygous for the DYT1-related p.Glu303del or p.Gly318Ser torsinA variant. All affected individuals presented with global developmental delays and contractures in multiple joints including elbows, wrists, fingers and toes. Contractures improved over time, but they still suffered from moderate to severe motor and intellectual deficits. Tremor, increased muscle tone and strabismus were additional symptoms. Electromyography (EMG), nerve conduction studies and brain MRI scans were unremarkable.

Reichert et al. published a case of an infant with compound heterozygous p.Glu303del and p.Thr321Argfs*6 variants. The patient presented with similar symptoms including contractures in all extremities and severe psychomotor delay. Brain MRI did not reveal structural abnormalities. [27]

Isik and colleagues reported a patient with a homozygous p.Arg288* variant. The child had severe global developmental delays and congenital contractures and died of respiratory arrest at the age of 4.5 months [28].

3.3 TorsinA – an AAA+ ATPase

The *TOR1A* gene consists of five exons that encode a 332 amino acid (aa) protein, torsinA, with a molecular weight (MW) of about 37 kilodaltons (kDa) [3, 29]. *TOR1A* is expressed ubiquitously in human tissues [3]. TorsinA is located throughout the endoplasmic reticulum (ER) and the nuclear envelope (NE) and is linked to the membranes of these organelles via its N-terminal hydrophobic amino acid-sequences [30-32].

TorsinA belongs to the AAA+ ATPase protein superfamily (ATPases Associated with various cellular Activities). AAA+ ATPases share an ATPase domain [3, 33-35] with strictly conserved motifs including a Walker A motif (for ATP binding), a Walker B motif (for ATP hydrolysis) and sensor 1, 2 domains (for ATP binding and hydrolysis) [36-40]. AAA+ ATPases form oligomeric, often hexameric rings and use the energy of ATP hydrolysis for a variety of functions such as unfolding, remodeling or disassembly of target proteins [41, 42]. Of note, torsinA lacks the catalytic arginine residue needed for ATP hydrolysis [43-45]. TorsinA forms complexes with lamina-associated peptide 1 (LAP1) and luminal domain-like LAP1 (LULL1), which contain arginine fingers projecting into

the active site of bound torsinA allowing its activation [46, 47]. LAP1 is located in the nuclear envelope whereas LULL1 is spread throughout the endoplasmic reticulum and nuclear envelope [43].

In addition to torsinA, there are four other known torsins in humans: torsinB, torsin2, torsin3 and torsin4 [3, 48]. Since torsin4 lacks the torsin defining ER targeting sequence, it is not generally accepted as a member of this protein family [48]. Of all torsins, torsinB shows highest similarity to torsinA (about 71 % of their amino acid sequences are similar or identical) [29].

3.4 Current understanding of torsinA's cellular function

3.4.1 TorsinA as a regulator of LINC complex assembly

The linker of nucleoskeleton and cytoskeleton (LINC) complex is a structure spanning the lumen of the nuclear envelope and provides a mechanical connection between the cytoskeleton and the nucleoskeleton. It is involved in various processes including movement of the nucleus, nuclear shaping and chromosome positioning [49-51]. It is composed of inner nuclear membrane SUN (Sad1/UNC84 homology) domain proteins and outer nuclear membrane KASH (Klarsicht/ANC-1/Syne homology) domain proteins interacting with each other in the lumen of the NE [52-54]. TorsinA has been reported to be involved in regulation of LINC complex assembly: TorsinA interacts directly with the KASH domain proteins nesprin (nuclear envelope spectrin repeat)-1, -2 and -3 and depletion or accumulation of torsinA alters the subcellular localization of nesprin-3, giant nesprin-2 (nesprin-2G) and SUN domain protein SUN2 [54-59].

3.4.2 TorsinA-dependent LINC complex formation and cell migration

Migration of fibroblasts requires actin dependent rearward movement of the nucleus which places the centrosome between the nucleus and the leading edge of the polarizing cell [60-62]. Further studies revealed that LINC complex proteins nesprin-2G and SUN2 as well as actin cables are essential for rearward movement of the nucleus, and thus for effective fibroblast migration [63]. Mechanistically, nuclear envelope proteins nesprin-2G, SUN2 and retrogradely moving dorsal actin cables form linear arrays called transmembrane actin associated nuclear (TAN) lines [63]. TorsinA and LAP1 are required for the assembly and persistence of these TAN lines, as well as the retrograde movement of

perinuclear actin cables, making torsinA the key regulator of efficient fibroblast migration [64].

3.4.3 TorsinA in nuclear envelope morphology and nucleo-cytosolic transport

In torsinA deficient mouse neurons (*Tor1a* knockout or homozygous p.Glu303del knock-in) a “blebbing” of the inner nuclear membrane into the perinuclear space was observed [65]. This phenotype could be replicated in other organisms with depleted torsinA homologues including *C. elegans* and *D. melanogaster* [59, 66]. Functional consequences of these blebs have remained elusive; however, this observation emphasizes the importance of torsinA for nuclear envelope morphology.

Nucleo-cytosolic transport is another nuclear envelope-related process that is impaired by torsinA malfunction. Nucleoporin localization and transport kinetics through the nuclear pore complex (NPC) are impaired in *C. elegans* lacking a functional torsinA homologue [59]. Studies in conditional *Tor1a* knockout mice neurons supported these findings [67]. Furthermore, torsinA has been shown to mediate NE trafficking of large ribonucleoprotein granules required for synapse development in *D. melanogaster* [66].

3.4.4 Other possible roles for torsinA in cell function

Several studies explored possible effects of torsinA on protein quality control and chaperone activity which is a *bona fide* function of an AAA+ ATPase. Indeed, torsinA’s chaperone-like behavior was demonstrated *in vitro* and *in vivo* [68, 69]. Moreover, torsinA is involved in ER-associated degradation (ERAD) and modulation of cellular susceptibility to ER stress [69, 70].

Other studies suggested torsinA to be required for synaptic vesicle recycling through binding snapin, a protein mediating synaptic vesicle docking [71, 72]. TorsinA was also shown to control stability of stonin-2, another essential protein in synaptic vesicle recycling [73, 74]. Consistent with these observations, the pool of recycling vesicles was decreased and exocytosis was increased in hippocampal neurons from homozygous *Tor1a* p.Glu303del knock-in mice [75].

Finally, torsinA may play a role in lipid metabolism. Conditional *Tor1a* knockout in mouse hepatocytes led to accumulation of lipid droplets in the ER and reduced VLDL biosynthesis and secretion, resulting in severe steatohepatitis [76]. Supporting these

findings, torsinA was found to act as a suppressor of the phosphatidic acid phosphatase lipin, which is important for the balance between lipid storage and membrane synthesis [77].

4 Material and methods

4.1 Materials

4.1.1 Laboratory equipment

-80 °C freezer: HERA freeze (Heraeus, Buckinghamshire, UK); U41085 Ultra Low Freezer (New Brunswick Scientific, Edison, NJ, USA)

37 °C incubation hood: Certomat H (B. Braun Biotech International, Berlin, Germany)

37 °C incubator for bacterial cultures: Heraeus Instruments (Heraeus)

Cell culture incubator: BBD 6220 (Heraeus)

Centrifuges: 5417, 5415R (Eppendorf, Hamburg, Germany); ROTINA 420R (Andreas Hettich GmbH & Co.KG, Tuttlingen, Germany), 6K15 (Sigma Laborzentrifugen, Osterode am Harz, Germany)

Detection system for WB: Odyssey Fc Imaging System (LI-COR Biosciences, Lincoln, USA)

Gel electrophoresis (nucleic acids) chamber: HE99X-15-1.5 gel chamber (Hoefer, Holliston, MA, USA)

Gel electrophoresis (nucleic acids) power supply: PS 3000 (Hoefer)

Gel electrophoresis (protein) chamber: SDS Mini-PROTEAN[®] Tetra Vertical Electrophoresis Cell (Bio-Rad, Hercules, CA, USA)

Gel electrophoresis (protein) power supply: PowerPac[™] HC High-Current Power Supply (Bio-Rad)

Gel documentation system: Intas GDS (Intas Science Imaging Instruments, Göttingen, Germany)

Laminar airflow cabinet (BDK, Sonnenbühl-Genkingen, Germany)

Microplate reader: TriStar LB 941 (Berthold Technologies, Bad Wildbad, Germany)

Microscope for immunofluorescence detection: FLUOVIEW FV1000 confocal laser scanning microscope (Olympus, Shinjuku, Tokio, Japan)

Microscope for cell culture assays: CKX53 microscope (Olympus), equipped with Moti-cam 10 camera (Motic, Hong Kong, China)

Precision balance: PRS 620-3N (Kern&Sohn, Balingen, Germany)

Shaker: Certomat R (B. Braun Biotech International), ST 5 (Ingenieurbüro CAT M. Zipperer, Ballrechten-Dottingen, Germany)

Spectrophotometer: Nanodrop ND-1000 (PeqLab, Erlangen, Germany)

Thermocycler: Mastercycler personal (Eppendorf, Hamburg, Germany); MJ Mini Thermal Cycler (Bio-Rad)

Thermoshaker: BioShake iQ (Quantifoil Instruments, Jena, Germany)

Western blot transfer system: Trans-Blot Turbo Transfer System (Bio-Rad)

pH meter: HI-9321 microprocessor pH Meter (Hanna Instruments Deutschland, Vöhringen, Germany)

Pipets: Pipetman Classic 20 µl, 200 µl, 1.000 µl (Gilson, Middleton, WI, USA), Eppendorf research plus 10 µl (Eppendorf), Pipet-Aid XP (Drummond Scientific Company, Broomall, PA, USA)

qRT-PCR cycler: CFX Connect Real-Time System (Bio-Rad)

Software: EndNote (Clarivate Analytics, London, UK); FV10-ASW 1.3 (Olympus); Image Studio (LI-COR Biosciences); Illustrator CS6 (Adobe, San José, CA, USA); Microsoft 365 (Microsoft Corporation, Redmond, WA, USA); Motic Images Plus 2.0 (Motic); Photoshop CS6 (Adobe); Python 2.7.9 (Python Software Foundation, DE, USA); The PyMOL Molecular Graphics System, Version 1.8.2.0 (Schrödinger, LLC).

4.1.2 Chemicals

If not otherwise indicated, all chemicals were purchased from Roth (Carl Roth GmbH + Co. KG, Karlsruhe, Germany) or Sigma-Aldrich (St. Louis, MO, USA). Exceptions are the following: Agarose (universal, peqGOLD molecular biology grade, VWR international, Radnor, PS, USA); VECTASHIELD Antifade Mounting Medium with DAPI (Vector Laboratories, Burlingame, CA, USA); Horse Serum (Invitrogen, Carlsbad, CA, USA).

4.1.3 Molecular biology kits and enzymes

The following molecular biology kits were used:

NucleoSpin Gel and PCR Clean-up (MachereyNagel, Düren, Germany); NucleoBond PC 500 (MachereyNagel); RNeasy Mini Kit (Qiagen, Venlo, Netherlands); QuantiTect Reverse Transcription Kit (Qiagen); Lipofectamine[®] 2000 transfection reagent (Invitrogen); JetPEI[®] (Polyplus, Illkirch, France); Dual-Luciferase[®] Reporter Assay (Promega, Madison, WI, USA).

The following enzymes (and specific buffers) were used:

Restriction endonucleases:

Restriction endonucleases were used together with Cut Smart Buffer, all purchased from New England Biolabs (Ipswich, MA, USA):

- *EcoRI*-HF
- *SalI*-HF
- *HindIII*-HF
- *DraIII*
- *XhoI*

Polymerases:

- colony polymerase chain reaction (PCR) and exon amplification:
DreamTaq Hot Start Green PCR Master Mix (Thermo Fisher Scientific, Waltham, MA, USA)
- Real-time qRT-PCR:
SsoAdvanced Universal SYBR Green Supermix (Bio-Rad)
- all other PCRs:
AccuPrime[™] Pfx DNA Polymerase with AccuPrime 10x reaction buffer (Invitrogen)

Ligase:

- T4 DNA Ligase with T4 DNA Ligase buffer (New England Biolabs)

Reverse transcriptase:

- Quantiscript Reverse Transcriptase (Qiagen)

4.1.4 Oligonucleotides

If not otherwise stated, primers were designed using the web tool Primer3 [78-80] (chapter 7.7.3 - Tools for primer design and cloning). All oligonucleotide primers were synthesized by Metabion (Martinsried, Germany).

4.1.4.1 Oligonucleotides for detection of *TOR1A* variants

Table 1: Oligonucleotides for detection of *TOR1A* variants

Oligonucleotide primer	Sequence 5'-3'
<i>TOR1A_E1_F</i>	TTTCCGGAAGCAAAACAGGG
<i>TOR1A_E1_R</i>	ATCCTCCATTCTCCATGCC
<i>TOR1A_E2_F</i>	GCAGTACTTGAGGTTTCGCA
<i>TOR1A_E2_R</i>	CGGGCTCACTCATTCAACA
<i>TOR1A_E34_F</i>	GGTCTGTAAGTGAAGCTGCG
<i>TOR1A_E34_R</i>	TTCCCCTCATGACTCGGAAG
<i>TOR1A_E5_F</i>	TGTGTGTGGCATGGATAGGT
<i>TOR1A_E5_R</i>	CAGGGAAAGGAGCTGGGG

4.1.4.2 Oligonucleotides for cDNA amplification

Table 2: Oligonucleotides for cDNA amplification

Oligonucleotide primer	Sequence 5'-3'
<i>EcoRI_TOR1A_F</i>	GCAGGAATTCCGCCACCCATGAAGCTGGGCCGGGCC
<i>Sall_TOR1A_R</i>	CGAGGTCGACTGATCATCGTAGTAATAATCTAACTTGGTG
<i>EcoRI_LAP1_F</i>	GCCCGAATTCTGATGGCCGGGCGACGGGCGGCCGGGCAGA
<i>XhoI_LAP1_R</i>	GTACCTCGAGATTATAAGCAGATGCCCTTTTCAGGGC
<i>EcoRI_LULL1_F</i>	GCCCGAATTCTGATGGCCGACAGTGGACTTAG
<i>XhoI_LULL1_R</i>	GTACCTCGAGATTAGAAAAGGCACCCCTGTTC

4.1.4.3 Oligonucleotides for site-directed mutagenesis

Table 3: Oligonucleotides for site-directed mutagenesis

Oligonucleotide primer	Sequence 5'-3'
<i>EcoRI_TOR1A_Kozak_WT_F</i>	GCAGGAATTCCGGTCCGGGCATGAAGCTGGGCCGGGCC
<i>EcoRI_TOR1A_Kozak_Mut_F</i>	GCAGGAATTCCGGTCCGTGCATGAAGCTGGGCCGGGCC
<i>Sall_TOR1A_Arg288*_R</i>	CGAGGTCGACTGGGACTGCATTTCCACTCGGATAC
<i>TOR1A_Glu171Gln_F</i>	AGGTCCATCTTCATATTTGATCAAATGGATAAGATGCATGCAG
<i>TOR1A_Glu171Gln_R</i>	CTGCATGCATCTTATCCATTTGATCAAATATGAAGATGGACCT
<i>TOR1A_Ser112Arg_F</i>	GCACCGGCAAAAATTTCTGCAGAAAAATCATCGCAGAGAATA-TTTACG
<i>TOR1A_Ser112Arg_R</i>	CGTAAATATTCTCTGCGATGATTTTTCTGACGAAATTTTT-GCCGGTGC
<i>pGL4.26_Kozak_WT_F</i>	TTCCAGCTTGGCAATCCGGTACTGTTGGTGGTCCGGGCATG-GAAGATGCCAAAAACATTAAGAAGG
<i>pGL4.26_Kozak_WT_R</i>	CCTTCTTAATGTTTTTGGCATCTTCCATGCCCGGACCACC-AACAGTACCGGATTGCCAAGCTGGAA

pGL4.26_Kozak_MUT_F	TTCCAGCTTGGCAATCCGGTACTGTTGGTGGTCCGTGCATG- GAAGATGCCAAAAACATTAAGAAGG
pGL4.26_Kozak_MUT_R	CCTTCTTAATGTTTTGGCATCTTCCATGCACGGACCACCA- ACAGTACCGGATTGCCAAGCTGGAA
pGL4.26_RV_Primer3	CTAGCAAATAGGCTGTCCC
pGL4.26_SDM_R	TCCTTGTCGATGAGAGCGTT

4.1.4.4 Oligonucleotides for qRT-PCR

Table 4: Oligonucleotides for qRT-PCR

Oligonucleotide primer	Sequence 5'-3'
<i>TOR1A</i> _qRT-PCR_F	CCCAAGAAACCTCTCACGCT
<i>TOR1A</i> _qRT-PCR_R	CCCAACTGTAAGTATCCTTGT
<i>GAPDH</i> _qRT-PCR_F	TCCCTGAGCTGAACGGGA
<i>GAPDH</i> _qRT-PCR_R	GGAGGAGTGGGTGTCGCT

4.1.4.5 Oligonucleotides for plasmid sequencing

Table 5: Oligonucleotides for plasmid sequencing

Oligonucleotide primer	Sequence 5'-3'
CMV_F	CGCAAATGGGCGGTAGGCGTG
EGFP-N	CGTCGCCGTCCAGCTCGACCAG
pCMV_myc_F	GATCCGGTACTAGAGGAACTGAAAAAC
pCMV_myc_R	CTTTATTTGTGAAATTTGTGATGCTAT
LAP1_seq_F	CTGTCAGGAGCATACAAGAGG
LULL1_seq_F	ACTTAGGGAGCAGCTCTGTG
pGL4.26_RV_Primer3	CTAGCAAATAGGCTGTCCC
pGL4.26_SDM_R	TCCTTGTCGATGAGAGCGTT

4.1.5 Plasmids

Table 6: Overview of plasmids used in this study

Plasmids	Description	Supplier
pEGFP-N1	Plasmid features: <ul style="list-style-type: none"> ▪ Multiple cloning site (MCS) ▪ Human cytomegalovirus (CMV) promoter ▪ Enhanced green fluorescent protein (EGFP) gene downstream of the MCS ▪ <i>E. coli</i> replication origin pUC for propagation in <i>E. coli</i> ▪ Kanamycin/neomycin resistance gene 	Clontech
pEGFP-N1-TOR1A-wt	pEGFP-N1 plasmid, containing <i>TOR1A</i> wild type (wt) complementary DNA (cDNA) sequence and a standard Kozak sequence, inserted in frame with the EGFP sequence using <i>EcoRI</i> and <i>Sall</i> sites.	This study

pEGFP-N1-Arg288*	pEGFP-N1 plasmid, containing a truncated <i>TOR1A</i> cDNA sequence (all bases after position 861 were removed) and a standard Kozak sequence, inserted in frame with the EGFP sequence using <i>EcoRI</i> and <i>SalI</i> sites.	This study
pEGFP-N1-Ser112Arg	pEGFP-N1 plasmid, containing <i>TOR1A</i> cDNA sequence including c.336C>A and c.339G>A variants and a standard Kozak sequence, inserted in frame with the EGFP sequence using <i>EcoRI</i> and <i>SalI</i> sites.	This study
pEGFP-N1-Glu171Gln	pEGFP-N1 plasmid, containing <i>TOR1A</i> cDNA sequence including c.511G>C mutation and a standard Kozak sequence, inserted in frame with the EGFP sequence using <i>EcoRI</i> and <i>SalI</i> sites.	This study
pEGFP-N1-Kozak-wt	pEGFP-N1 plasmid, containing <i>TOR1A</i> wt cDNA sequence and the <i>TOR1A</i> Kozak sequence, inserted in frame with the EGFP sequence using <i>EcoRI</i> and <i>SalI</i> sites.	This study
pEGFP-N1-Kozak-mut	pEGFP-N1 plasmid, containing <i>TOR1A</i> wt cDNA sequence and the <i>TOR1A</i> Kozak sequence including the c.-3G>T variant, inserted in frame with the EGFP sequence using <i>EcoRI</i> and <i>SalI</i> sites.	This study
pGL4.26	Plasmid features: <ul style="list-style-type: none"> ▪ MCS ▪ Minimal promoter ▪ <i>Luc2</i> (firefly luciferase) reporter gene ▪ <i>ColE1</i>-derived plasmid replication origin for propagation in <i>E. coli</i> ▪ Ampicillin resistance gene 	Promega
pGL4.26-Kozak-wt	pGL4.26 plasmid, containing the <i>TOR1A</i> Kozak sequence upstream of the AUG initiation codon, inserted using <i>HindIII</i> and <i>DraIII</i> sites.	This study
pGL4.26-Kozak-mut	pGL4.26 plasmid, containing <i>TOR1A</i> Kozak sequence upstream of the AUG initiation codon including the c.-3G>T variant, inserted using <i>HindIII</i> and <i>DraIII</i> sites.	This study
pRL-TK	Plasmid features: <ul style="list-style-type: none"> ▪ MCS ▪ Herpes simplex virus thymidine kinase (HSV-TK) promoter ▪ <i>Rluc</i> (<i>Renilla</i> luciferase) reporter gene ▪ <i>E. coli</i> replication origin pUC for propagation in <i>E. coli</i> ▪ Ampicillin resistance gene 	Promega

pCMV-HA-N	Plasmid features: <ul style="list-style-type: none"> ▪ MCS ▪ CMV promoter ▪ HA epitope gene upstream of the MCS ▪ <i>E. coli</i> replication origin pUC for propagation in <i>E. coli</i> ▪ Ampicillin resistance gene 	Clontech
pCMV-HA-N-LAP1	pCMV-HA-N, containing the <i>TOR1AIP1</i> cDNA sequence in frame with the HA epitope, inserted using <i>EcoRI</i> and <i>XhoI</i> sites.	This study
pCMV-HA-N-LULL1	pCMV-HA-N, containing the <i>TOR1AIP2</i> cDNA sequence in frame with the HA epitope, inserted using <i>EcoRI</i> and <i>XhoI</i> sites.	This study

4.1.6 Antibodies

4.1.6.1 Primary antibodies

Table 7: Primary antibodies

Primary antibody	Supplier	Host	Dilution	Used blocking solution
anti-α-tubulin	Abcam	mouse	IF: 1:1,000	5 % HS in PBS
anti-α-tubulin	Cell Signaling Technology	rabbit	WB: 1:1,000	5 % BSA in PBS
anti-GAPDH	Merck Millipore	mouse	WB: 1:500	10 % milk in TBS-T
anti-GFP	Abcam	rabbit	WB: 1:10,000	5 % BSA in PBS
anti-HA	Roche	rat	IF: 1:500	5 % HS in PBS
anti-LC3A (NB100-2331)	Novus Biologicals	rabbit	WB: 1:1,000	5 % milk in TBS-T
anti-PDI	Enzo Biochem. Inc.	mouse	IF: 1:500	5 % HS in PBS
anti-pericentrin	Abcam	rabbit	IF: 1:2,000	5 % HS in PBS
anti-torsinA	Cell Signaling Technology	mouse	WB: 1:200	5 % milk in TBS-T

BSA: bovine serum albumin; HS: horse serum; IF: immunofluorescence; PBS: phosphate buffered saline; TBS-T: Tris buffered saline with Tween20; WB: western blot

4.1.6.2 Secondary antibodies

Table 8: Secondary antibodies

Secondary antibody	Supplier	Host	Dilution
IRDye 680CW anti-mouse IgG	LI-COR Biosciences	donkey	WB: 1:10,000
IRDye 680CW anti-rabbit IgG	LI-COR Biosciences	donkey	WB: 1:10,000
IRDye 800CW anti-mouse IgG	LI-COR Biosciences	donkey	WB: 1:10,000
IRDye 800CW anti-rabbit IgG	LI-COR Biosciences	donkey	WB: 1:10,000
Alexa Fluor 488-conjugated anti-mouse IgG AffiniPure	Thermo Fisher Scientific	goat	IF: 1:500
Alexa Fluor 488-conjugated anti-rabbit IgG AffiniPure	Thermo Fisher Scientific	goat	IF: 1:500
Alexa Fluor 594-conjugated anti-mouse IgG AffiniPure	Thermo Fisher Scientific	goat	IF: 1:500
Alexa Fluor 594-conjugated anti-rat IgG	Thermo Fisher Scientific	goat	IF: 1:500

IF: immunofluorescence; WB: western blot

4.1.7 *E. coli* strains**Table 9: *E. coli* strains**

Strain	Genotype
DH5α	F ⁻ ϕ 80lacZ Δ M15 Δ (lacZYA-argF)U169 <i>recA1 endA1 hsdR17</i> (rK ⁻ , mK ⁺) <i>phoA supE44 λ^- thi-1 gyrA96 relA1</i>
K802	F ⁻ <i>e14⁻ (McrA⁻) lacY1</i> or Δ (lac)6 <i>glnV44 galK2 galT22 rfbD1 metB1 mcrB1 hsdR2 (rK⁻ mK⁺)</i>

4.1.8 Mammalian cell lines

Human embryonic kidney 293 (HEK293) and Henrietta Lacks (HeLa) cell lines were obtained from ATCC (LGC Standards, Wesel, Germany). Human dermal fibroblasts of patients and non-disease control individuals were obtained from the biobank of the Friedrich-Baur-Institute (MTCC, Munich tissue culture Collection).

4.2 Methods

4.2.1 *In silico* prediction tools

PROVEAN [81], SIFT [82], PolyPhen-2 [83], CADD [84], LRT [85], SNAP2 [86], MutationAssessor [87], VEST3 [88], MutationTaster2 [89], PMut [90], GERP++ [91], PhastCons100way score [92], TraP [93], DDIG [94], DANN [95], Fathmm-MLK [96], PredictSNP2 [97] and PhD-SNP^g [98] were used to evaluate the pathogenetic relevance of p.Ser112Arg and c.339G>A variant *in silico* (chapter 7.7.1 - *In silico* prediction tools).

For estimation of allele frequencies in the general population, the following databases were used: Exome Variant Server (NHLBI GO Exome Sequencing Project (ESP), Seattle, WA, USA, [02/2022]), 1000G [99] and gnomAD-Exomes [100] (chapter 7.7.2 - Genome and exome databases).

4.2.2 Microbiological methods

4.2.2.1 Culturing of *E. coli*

E. coli were cultured in Luria-Bertani (LB) medium containing antibiotics according to the resistance gene of the transformed plasmid. Culturing was performed at 37 °C under continuous shaking at 200 rpm. In order to obtain single colonies, cells were plated on LB agar plates containing antibiotics according to the resistance gene.

LB medium:

- 1.0 % bacto-tryptone
- 1.0 % NaCl
- 0.5 % bacto-yeast extract
- pH: 7.0

For agar plate preparation, 2 % agar was added to the LB medium. Antibiotics were used in following concentrations: ampicillin (100 µg/ml), kanamycin (50 µg/ml).

4.2.2.2 Preparation of competent cells

100 ml of LB medium was inoculated with 100 µl of *E. coli* from glycerol stocks and incubated at 37 °C under continuous shaking until OD₆₀₀ reached 0.4-0.6. Cells were pelleted at 3,500 rpm for 15-20 min at 4 °C. The pellet was resuspended in 30 ml of ice-cold TFB-I and centrifuged at 3,500 rpm for 5 min. at 4 °C. *E. coli* were then resuspended in ice-cold TFB-II. Aliquots were stored at -80 °C.

TFB-I:

- 30 mM K⁺-acetate
- 100 mM KCl
- 50 mM MnCl₂
- 15 % glycerol
- pH: 5.8

TFB-II:

- 10 mM MOPS/NaOH, pH: 7.0
- 75 mM CaCl₂
- 10 mM KCl
- 15 % glycerol

4.2.2.3 Plasmid transformation

50 µl of chemically competent *E. coli* were thawed on ice for 10 min. 5 µl of the ligation solution were added and incubated on ice for 20 min. Afterwards a heat shock was set for 1 min at 42 °C and the solution was chilled for 5 min on ice. 1 ml of LB medium was added and the suspension was incubated at 37 °C for 1 h. The cells were pelleted by centrifugation at 13.000 rpm for 1 min. *E. coli* were resuspended in 100 µl of fresh LB medium and plated on LB agar plates containing antibiotics according to the resistance gene on the transformed plasmid. The plates were incubated for 16 h at 37 °C.

4.2.2.4 Isolation of plasmid DNA from *E. coli*

4.2.2.4.1 Miniprep

Buffers S1, S2 and S3 were contained in the plasmid purification kit NucleoBond PC 500. 5 ml of LB medium (containing antibiotics corresponding to the resistance gene of the transformed plasmid) were inoculated with one colony of *E. coli* and incubated for 16 h at 37 °C shaking at 200 rpm. 2 ml of the bacteria suspension were centrifuged for 5 min at 14,000 rpm. The pellet was resuspended in 250 µl of S1 buffer and incubated for 10 min at room temperature (rt). 250 µl of S2 buffer were added and the mixture was gently shaken for 5 min. Afterwards, 350 µl of S3 buffer were added and the solution was incubated on ice for 10 min. After centrifugation for 10 min at 14,000 rpm and 4 °C, the supernatant was collected and 600 µl of isopropanol were added. The solution was centrifuged for 30 min at 4 °C and 14,000 rpm. The pellet was washed two times in 500 µl ethanol for 5 min at 14,000 rpm and 4 °C. The pellet was then dried at 50 °C and resuspended in the appropriate volume of TE buffer.

TE buffer:

- 10 mM Tris-HCl
- 1 mM EDTA
- pH: 8.0

4.2.2.4.2 Maxiprep

250 ml of LB medium containing antibiotics corresponding to the resistance gene of the transformed plasmid were inoculated with 150 µl of the 2 ml culture described in the previous section. The culture was incubated for 16 h at 37 °C under shaking at 200 rpm. The bacteria were pelleted the next day for 15 min at 3,500 rpm and 4 °C. The isolation of the plasmid DNA was performed using the NucleoBond PC 500 kit according to manufacturer's instructions.

4.2.3 Nucleic acid methods**4.2.3.1 Agarose gel electrophoresis**

Agarose gel electrophoresis was performed for qualitative and quantitative DNA analysis as well as for purification of DNA fragments. 1 % agarose was added to 1xTAE buffer and the solution was boiled until the agarose was completely dissolved. The solution was cooled down to around 50 °C, ethidium bromide was added to a final concentration of 0.1 µg/ml and the gel was poured into the tray with a properly placed comb. After solidification, gels were put into horizontal electrophoresis chambers filled with 1x TAE buffer.

Before loading samples onto the gel, 6x DNA loading dye (Thermo Fisher Scientific) was added to the nucleic acid solution (except PCRs performed with DreamTaq Hot Start Green PCR Master Mix). 1 kb (GeneRuler™ 1 kb Plus DNA ladder, Thermo Fisher Scientific) or 100 bp ladders (GeneRuler™ 100 bp DNA ladder, Thermo Fisher Scientific) were used as size standards. Gels were run at 140 V for 60 min. The DNA was visualized by ultraviolet (UV) light and pictures were captured with Intas gel documentation system.

TAE:

- 0.049 M Tris
- 2 mM EDTA
- pH: 8.5

4.2.3.2 Gel purification

Gel purification was performed with the aid of NucleoSpin Gel and PCR Clean-up kit according to manufacturer's instruction. In short, gel blocks with the desired DNA band were cut out under UV light control and dissolved in a proprietary buffer at 50 °C.

Afterwards the DNA was loaded on a column, washed and eluted with the required amount of TE buffer.

4.2.3.3 Quantification of DNA and RNA samples

The concentrations of genomic or plasmid DNA, PCR products and RNA were measured using a NanoDrop ND-1000 spectrophotometer.

4.2.3.4 Polymerase Chain Reaction (PCR)

4.2.3.4.1 Colony PCR

Before starting liquid cultures from *E. coli* colonies from agar plates, colony PCR was used to ensure that selected colonies contained the plasmid and DNA insert of interest. Using a sterile toothpick, a small portion of the colonies was transferred into the reaction mix and subjected to PCR using appropriate oligonucleotide primer sets.

Primer sets were designed in two different ways:

The first method was based on one primer binding to the insert and the other one to the flanking plasmid DNA. An amplicon was only generated if the desired DNA fragment was present.

The second method involved primers flanking the insert on both sides. An amplicon corresponding to the length of the inserted DNA fragment indicated successful insertion.

Table 10: Reaction mix for colony PCR

Components	Amount per reaction
Hot Start Green master mix	13 μ l
Forward primer	1 μ l
Reverse primer	1 μ l
Template	Inoculation with <i>E. coli</i> colony
Nuclease free water	ad 25 μ l
Total reaction volume	25 μ l

Table 11: PCR program for colony PCR

Temperature	Time	Cycles
95 °C	6 min	1x
95 °C	30 sec	40x
50 °C	30 sec	
72 °C	90 sec	
72 °C	7 min	1x

4.2.3.4.2 Amplification of genomic DNA

Genomic DNA samples from patients and their relatives were used to amplify exons of *TOR1A* including adjacent introns and UTR sequences. PCR products were run on agarose gels for quality control and were then purified for sequencing analysis as described above.

Table 12: Reaction mix for amplification of genomic DNA

Components	Amount per reaction
Hot Start Green master mix	13 µl
Forward primer	1 µl
Reverse primer	1 µl
Genomic DNA	100-500 ng
Nuclease free water	ad 25 µl
Total reaction volume	25 µl

Table 13: PCR program for exon amplification of genomic DNA

Temperature	Time	Cycles
95 °C	6 min	1x
95 °C	30 sec	40x
57 °C	30 sec	
72 °C	60 sec	
72 °C	7 min	1x

4.2.3.4.3 Site-directed mutagenesis

Site directed mutagenesis with mismatch primers was performed using overlap extension PCR [101]. Oligonucleotide primers used for introduction of sequence variants are listed in chapter 4.1.4.3 (Oligonucleotides for site-directed mutagenesis) and were designed using QuikChange[®] Primer Design (Agilent, Santa Clara, CA, USA) (chapter 7.7.3 - Tools

for primer design and cloning). The outer primers contained restriction sites for cloning of the resulting fragment into the target plasmids.

4.2.3.4.4 Extraction of RNA

Total RNA was isolated from patient derived fibroblasts, HEK293 and HeLa cells (chapter 4.1.8 - Mammalian cell lines). Cells were grown until confluency on 10 cm dishes, growth medium was discarded, and cells were lysed with 750 μ l of TRIzol™ (Invitrogen) reagent by gently pipetting the lysate up and down. After transferring the lysate to a 1.5 ml tube and incubation for 5 min at rt, 75 μ l of chloroform was added, followed by another 2 min incubation at rt. The lysate was then centrifuged at 13,000 rpm for 15 min at 4 °C before the colorless RNA-containing upper phase was transferred into a new tube. The RNA lysate was dissolved with equivalent amount of isopropanol. The following RNA purification was performed using the RNeasy® Mini kit (Qiagen) according to the manufacturer's manual.

4.2.3.4.5 Generation of cDNA

For cloning of expression constructs, full-length *TOR1A*, *TOR1AIP1* (encoding LAP1) and *TOR1AIP2* (encoding LULL1) cDNA was generated by reverse transcription of mRNA using the QuantiTect Reverse Transcription Kit (Qiagen) according to the manufacturer's instructions. *TOR1A* mRNA was used from total mRNA of human placenta cells included in the SMART™-RACE cDNA Amplification Kit (CLONTECH Laboratories, Inc., Palo Alto, CA, USA). *TOR1AIP1* mRNA was isolated from HEK293 cells and *TOR1AIP2* mRNA from HeLa cells. cDNA for real-time qRT-PCR analysis was generated using mRNA preparations from patient and control fibroblasts.

4.2.3.4.6 Real-time quantitative reverse transcription PCR (real-time qRT-PCR)

For quantification of *TOR1A* expression, Real-time qRT-PCR was performed using the SsoAdvanced Universal SYBR Green Supermix (2x). Samples were amplified in a 96-Well Optical Reaction Plate (Bio-Rad) using a CFX96 Real-Time System (Bio-Rad). To correct for sample-to-sample-variation, an endogenous control, *GAPDH*, was amplified with the target. The expression levels of *TOR1A* relative to *GAPDH* were calculated using the $2^{-\Delta\Delta CT}$ method [102]. Primers for *TOR1A* were designed according to the following requirements: length of amplified fragment: 150-250 bp, length of primer: around 20 bp, melting temperature: around 60 °C. Primer efficiency and specificity were checked by

PCR with fibroblast cDNA as template. *GAPDH* primers were adapted from previously published sequences [103, 104].

Table 14: Reaction mix for real-time qRT-PCR

Components	Amount per reaction
SsoAdvanced Universal SYBR Green Supermix (2x)	10 μ l
Forward primer	1 μ l
Reverse primer	1 μ l
cDNA (1:8 dilution)	2 μ l
RNAse free water	6 μ l
Total reaction volume	20 μ l

Table 15: PCR program for real-time qRT-PCR

Temperature	Time	Cycles
95 °C	30 sec	1x
95 °C	5 sec	40x
60 °C	30 sec	
65-95 °C in 0.5 °C increments	each step 5 sec	1x

4.2.3.5 Restriction digest

For cloning by restriction digest and ligation, restriction enzymes cutting at the desired sites were used to digest plasmid backbones and DNA inserts. If possible, restriction endonucleases producing “sticky-ends” were selected. Digestion was performed for 2 h at 37°C.

For testing identity of plasmid preparations, plasmids were digested with suitable restriction enzymes and analyzed by agarose gel electrophoresis. Successful transformation (and ligation) was monitored by detection of a specific pattern of DNA bands.

Table 16: Restriction digest reaction mix for testing plasmid identity

Components	Amount per reaction
DNA fragment (qualitative analysis)	500 ng
Restriction enzyme 1	20 units (U)
Restriction enzyme 2	20 U
NEB Cut Smart buffer	1 µl
ddH ₂ O	ad 10 µl
Total reaction volume	10 µl

Table 17: Restriction digest reaction mix for plasmid generation

Components	Amount per reaction
DNA fragment (cloning)	14 µg
Restriction enzyme 1	40 U
Restriction enzyme 2	40 U
NEB Cut Smart buffer	10 µl
ddH ₂ O	ad 100 µl
Total reaction volume	100 µl

4.2.3.6 Ligation

Ligation of restriction digested DNA fragments and plasmids was performed with T4 DNA ligase. The reaction mixture contained 100 ng of plasmid and an amount of insert DNA calculated with the following formula (size in bp):

$$m(\text{Insert}) = \frac{m(\text{empty plasmid}) * \text{size}(\text{insert}) * 3}{\text{size}(\text{plasmid})}$$

Table 18: Reaction mix for ligation

Components	Amount per reaction
Plasmid	100 ng
Insert	100 ng
T4 DNA ligase	1 µl
T4 DNA reaction buffer (10x)	1 µl
ddH ₂ O	ad 10 µl
Total reaction volume	10 µl

The reaction mix was pipetted at rt, put in an isolation box and incubated at 4 °C over night (o.n.).

4.2.3.7 Sanger sequencing

Purified DNA fragments were premixed with sequencing primers. Sequencing was performed by Eurofins Genomics GmbH (Ebersberg, Germany).

4.2.4 Mammalian cell culture

4.2.4.1 Propagation of cells

All cells were cultured in Dulbecco's Modified Eagle's medium (DMEM) (Gibco, Darmstadt, Germany) supplemented with 10 % fetal calf serum (FCS), 2 mM glutamine, 40 U/ml penicillin and 0.04 mg/ml streptomycin. All cell cultures were incubated at 37 °C in humidified atmosphere with 5 % CO₂.

4.2.4.2 Passage of cells

To passage adherent cells, medium was removed by vacuum suction and cells were washed with sterile phosphate buffered saline (PBS). Cells were detached by incubation in 0.05 % trypsin-EDTA for around 5 min at 37 °C. Cells were then suspended in fresh culture medium and re-plated following dilution in DMEM.

4.2.4.3 Transfection of cells

4.2.4.3.1 Transfection using Lipofectamine[®] 2000

Cells were cultured on 10 cm, 6-well or 24-well dishes and on cover slips (CS) until confluency of about 60 % for immunofluorescence microscopy or about 90 % for western blot analysis. Lipofectamine[®] 2000 transfection reagent was used according to manufacturer's instructions. To check transfection efficiency, empty pEGFP-N1 vector was co-transfected in western blot experiments. Cells were harvested or fixed 24 h after transfection.

4.2.4.3.2 Transfection using jetPEI[®]

Human dermal fibroblasts were grown on CS until confluency of around 60 %. JetPEI[®] transfection reagent was used according to manufacturer's instructions. Cells were fixed 24 h after transfection.

4.2.4.4 Harvesting of cells

Medium was removed by vacuum suction and cells were washed with sterile PBS. Adherent cells were mechanically scraped into ice cold PBS and transferred to a 1.5 ml tube. Afterwards, cells were pelleted by centrifugation (14,000 rpm, 5 min, 4 °C). Cell pellets were either used for protein isolation or stored at -80 °C.

4.2.4.5 Wound healing assay

Patients' and control fibroblasts were cultured in 35 mm μ -Dishes with 2-well culture inserts (IBIDI, Martinsried, Germany). After fibroblasts had reached confluency, the inserts were removed leaving a 500 μ m gap. Pictures were taken every 24 h using a CKX53 microscope equipped with a Moticam 10 camera.

4.2.4.6 Centrosome reorientation assay

For centrosome reorientation studies, human dermal fibroblasts were grown on cover slips until confluency. They were washed two times with PBS and serum starved for 24 h in serum free medium. A scratch was made using a 200 μ l pipet tip and cells were cultured another 3 h in standard culture medium containing 2 μ M lysophosphatidic acid (LPA). They were fixed and stained with anti-pericentrin and anti- α -tubulin antibodies [55]. Centrosomes were counted as positive orientated if they were located in the area between the nucleus and the edge of the wound [105].

4.2.4.7 Protein degradation and stability assays

4.2.4.7.1 Autophagy inhibition using bafilomycin A1

Twelve h post transfection, bafilomycin A1 was added at a final concentration of 0.1 μ M to the culture medium of HEK293 cells. Cells were harvested 12 h after application of the inhibitor. DMSO was used as a vehicle-only control.

4.2.4.7.2 Proteasome inhibition using MG132

Seven h post transfection, MG132 was added at a final concentration of 5 μ M to the culture medium of HEK293 cells. Cells were harvested 17 h after application of the inhibitor. DMSO was used as a vehicle-only control.

4.2.4.7.3 Cycloheximide chase experiment

Twenty-four h after transfection of HEK293 cells, cycloheximide was added to the culture medium at a final concentration of 20 μ g/ml. Cells were harvested 2, 4, 6 and 8 h after application of the inhibitor.

4.2.5 Protein methods

4.2.5.1 Protein isolation

Cell pellets were resuspended in lysis buffer using a 1,000 μ l pipet tip. After incubation at 95 °C for 5 min, the solution was homogenized using a 200 μ l pipet tip. After centrifugation for 5 min at 14,000 rpm and 4 °C, the supernatant was used for western blot analysis.

Lysis buffer:

- 10 mM Tris-HCl, pH: 7.4
- 1 % sodium dodecyl sulfate (SDS)

4.2.5.2 Protein quantification

All protein solutions were measured twice with a NanoDrop ND-1000 spectrophotometer using the absorption at 280 nm. The mean value of both measurements was used for further calculations.

4.2.5.3 SDS polyacrylamide gel electrophoresis of proteins (SDS-PAGE)

Samples for SDS-PAGE were prepared as follows:

Table 19: Sample preparation for SDS-PAGE

Components	Amount per slot
Protein	67 μ g
6x SDS loading dye	5 μ l
ddH ₂ O	ad 30 μ l
Total volume	30 μ l

Proteins were separated on 4-15 % SDS pre-cast gradient gels (Mini-PROTEAN TGX Precast Protein Gel; Bio-Rad) in a SDS Mini-PROTEAN[®] Tetra Vertical Electrophoresis Cell filled with running buffer. Voltage was set to 80 V until all proteins were run into the collecting gel, then voltage was increased to 120 V. PageRuler Prestained Protein Ladder (Thermo Fisher Scientific) was used as protein size marker.

SDS loading dye (6x):

- 20 mM Tris-HCl, pH: 6.8
- 6 % SDS
- 30 % glycerol
- 0.03 % bromphenol blue
- 5 % β -Mercaptoethanol

Running buffer:

- 25 mM Tris
- 192 mM glycine
- 0.1 % SDS

4.2.5.4 Western blotting

Western blotting was performed using the Trans-Blot Turbo Transfer System (Bio-Rad). Proteins were transferred on a 0.45 μm Low Fluorescence PVDF (LF PVDF) membrane (Bio-Rad) using the MIXED MW program according to the manufacturer's protocol. Membranes were immersed in methanol for 20 sec before use.

After the transfer, the membranes were blocked either in 5 % non-fat milk in Tris buffered saline with Tween20 (TBS-T) or in 5 % bovine serum albumin (BSA) in PBS depending on optimized conditions for the used primary antibodies. Afterwards, membranes were incubated o.n. at 4 °C in the primary antibody solution. Following three washes with TBS-T or PBS for 10 min, membranes were incubated in the secondary antibody solution in a dark chamber for 1 h at rt. After incubation, the previous washing steps were repeated. All washing and incubation steps were performed under gentle shaking.

For image acquisition and signal quantification, an Odyssey Fc Imaging System and ImageStudio software were used.

TBS-T:

- 10 mM Tris-HCl, pH: 7.4
- 140 mM NaCl
- 0.1 % Tween-20

4.2.6 Immunofluorescence microscopy

For immunofluorescence staining, cells were grown on glass cover slips and transfected as previously described. 24 h post transfection, medium was removed by vacuum suction and cover slips were washed with PBS. Cells were fixed in methanol at -20 °C. If not used for staining immediately, cover slips were stored in methanol at -20 °C.

After fixation, cover slips were washed three times for 5 min with PBS. Cells were blocked for 1 h at rt in 5 % horse serum (HS) in PBS and incubated in primary antibody solution (in 5 % HS in PBS) at 4 °C o.n. Following three washes in PBS, incubation with secondary antibodies (in 5 % HS in PBS) was performed for 1 h at rt in a dark chamber. After washing three times in PBS once more, cover slips were mounted in VECTASHIELD Antifade Mounting Medium with DAPI. Pictures were taken with an Olympus FLUOVIEW FV1000 confocal laser scanning microscope.

4.2.7 Dual luciferase reporter assay

pGL4.26 firefly luciferase vector was modified as described above in order to test effects of the *TORIA* Kozak sequence variant on gene expression. HEK293 cells were plated on

24-well plates (0.8×10^5 cells per well) and transfected with 200 ng of pGL4.26 construct and 2 ng of pRL-TK control vector. Luciferase expression was analyzed 24 h after transfection using the Dual-Glo[®] Luciferase Assay System on a TriStar LB 941 reader according to the manufacturer's instructions. Relative reporter activity was calculated by normalization of firefly luciferase activity to *Renilla* luciferase activity.

4.2.8 Statistical analysis

For quantification of results, means and standard deviations were calculated from at least three independent experiments. Statistical significance was determined with two-tailed Student's t-test. A P-value of <0.05 was considered as statistically significant (*), $P < 0.01$ was considered as statistically very significant (**) and $P < 0.001$ was considered as statistically highly significant (***)

5 Results

5.1 Identification of *TOR1A* variants in AMC patients

To search for new causes of AMC, a family with a presumed autosomal recessive, etiologically unresolved multiple congenital contracture syndrome (family A) was selected from the Friedrich-Baur-Institute collection of patients with neurogenetic diseases of unknown cause. Whole exome sequencing (WES) of the index patient's DNA revealed a homozygous *TOR1A* variant c.862C>T (p.Arg288*) which was the most plausible candidate under the assumption of recessive inheritance (Figure 1) (Table S1). Sanger sequencing of the *TOR1A* sequence using DNA samples from the similarly affected sibling and healthy parents confirmed the segregation of the mutated allele as an autosomal recessive trait (Figure 2, A). In an independent study, a collaborating group (Prof. Sébastien Moutton, Dijon, France) discovered an identical homozygous p.Arg288* *TOR1A* variant in an unrelated family (family B) with a strikingly similar clinical presentation. Sanger sequencing of the *TOR1A* gene in further family members (parents and affected sibling) was also consistent with autosomal recessive inheritance. The p.Arg288* variant was absent or present at only very low frequency in databases representing normal human genome variability (gnomAD, EVS, 1000G) (Table 20).

5.2 Sanger sequencing of patients with similar phenotypes

Thirty-five additional unrelated patients with genetically unresolved AMC were screened for *TOR1A* variants by Sanger sequencing. This analysis revealed one additional case (C-II:1, family C) carrying compound heterozygous *TOR1A* variants. Segregation studies using parental DNA samples revealed that a c.-3G>T variant in the 5'-untranslated region (UTR) resided on the maternal allele while a missense variant c.336C>A (p.Ser112Arg) and a synonymous variant c.339G>A affecting two adjacent codons were both paternally inherited (Figure 1) (Figure 2, B). All three variants were not detected or only detected at very low frequencies in the general population (represented by gnomAD, EVS, 1000G) (Table 20).

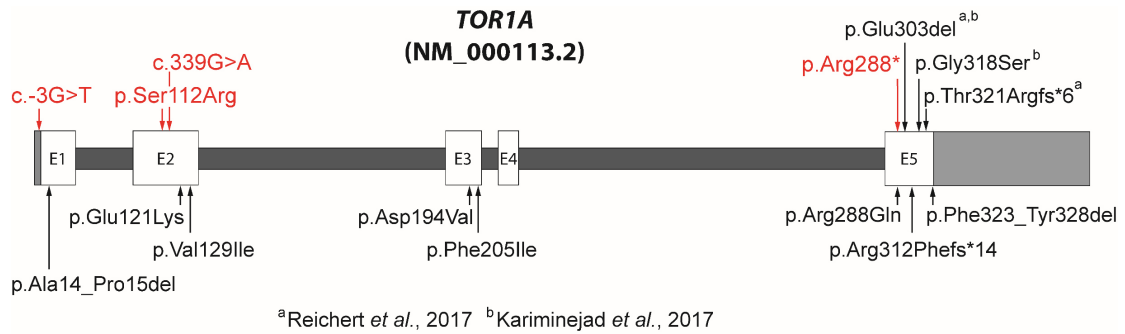


Figure 1: DYT1- and AMC-related variants in TOR1A

Schematic drawing of the exon structure of *TOR1A* (E1-E5: exons 1-5). Variants depicted above the graphic represent AMC variants [27, 106]. Variants identified in this study are printed in red. Variants depicted below the graphic represent DYT1 variants [3, 15-21].

Table 20: TOR1A variants and their frequencies in global databases

cDNA change	Amino acid change	EVS (allele number)	gnomAD exomes (allele number)	1000G (allele number)
c.-3G>T	-	0 (13,006)	0 (251,494)	0 (5,008)
c.336C>A	p.Ser112Arg	0 (13,006)	3.976e-6 (251,496)	0 (5,008)
c.339G>A	p.Lys113Lys	0 (13,006)	1.193e-5 (251,496)	0 (5,008)
c.862C>T	p.Arg288*	0 (13,006)	2.783e-5 (251,492)	0 (5,008)

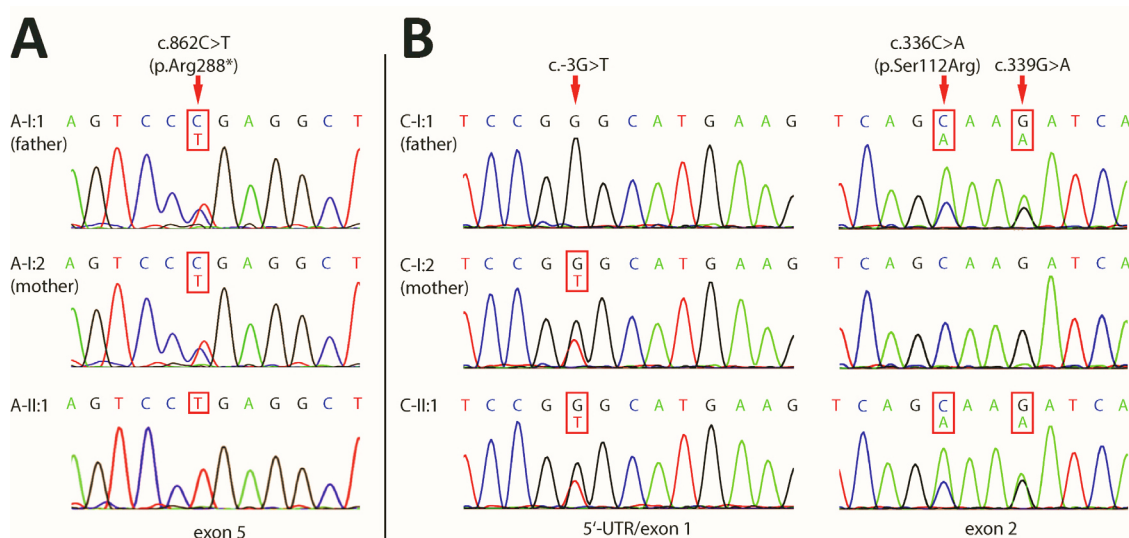


Figure 2: TOR1A variants identified in families A and C.

(A) Sanger sequencing chromatograms of patient A-II:1 and parents A-I:1 and A-I:2

A partial sequence of *TORIA* exon 5 is shown. The position of the c.862C>T variant is marked with a red arrow.

(B) Sanger sequencing chromatograms of patient C-II:1 and parents C-I:1 and C-I:2

Partial sequences of the *TORIA* 5'-UTR and exon 2 are shown. Positions of c.-3G>T, c.336C>A and c.339G>A variants are marked with red arrows.

5.3 *In silico* assessment of pathogenicity of identified variants

The p.Arg288* nonsense variant is expected to escape nonsense-mediated mRNA decay as it occurs in the last coding exon [107]. Instead, it is predicted to lead to C-terminal truncation of torsinA. This would result in a loss of α 7, α 8 helices and β 6, β 7 sheets including the sensor 2 domain, a structure essential for torsinA's ATPase function [39, 40, 108] (Figure 3).

The 5'-UTR variant c.-3G>T affects a highly conserved position in the vertebrate Kozak sequence and is, therefore, likely to interfere with translation of the *TORIA* mRNA [109-111]. Multiple sequence alignments (MSA) of *TORIA* Kozak sequences from several vertebrates confirm strict conservation of the guanine base at position -3 (Figure 4, A).

Variant c.336C>A (p.Ser112Arg) is located close to the Walker A motif, which is important for ATP binding (Figure 3) [37]. It is predicted to be deleterious or possibly disease causing by 12 out of 12 *in silico* prediction algorithms (Table S2). Multiple sequence alignments show that residue p.Ser112 is highly conserved in vertebrates and non-vertebrates (Figure 4, B).

The synonymous variant c.339G>A does not alter the amino acid sequence and is predicted to be benign or neutral by six out of eight *in silico* tools (Table S2). Splicing analysis with Human Splicing Finder [112] predicts a potential weak effect on an exonic splicing enhancer element. Because of the rather benign *in silico* predictions, the c.339G>A variant is considered less likely to contribute to the etiology of AMC and lower priority is given to further exploration of this variant.

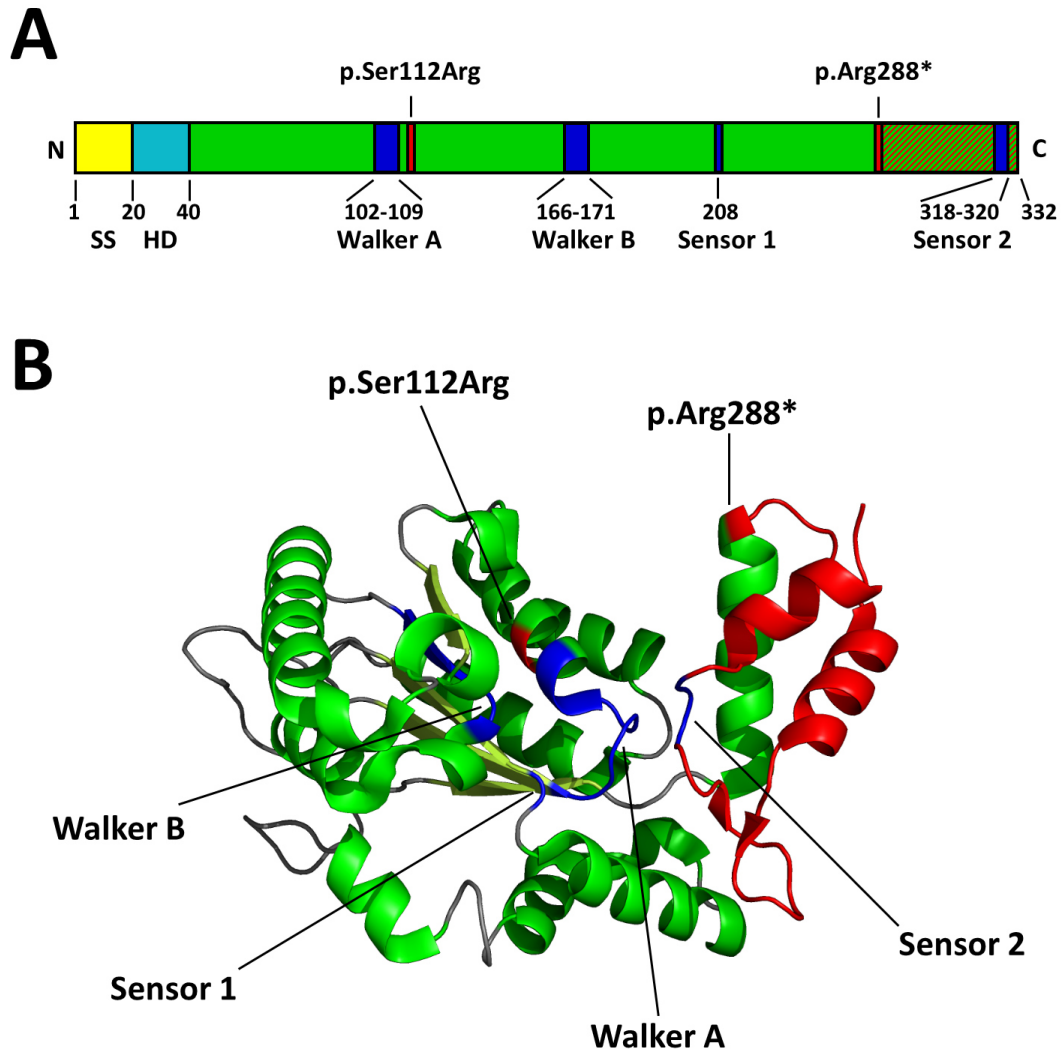


Figure 3: Primary and tertiary structures of torsinA

(A) Schematic representation of functional and structural units in torsinA

Signal sequence (SS): yellow; N-terminal hydrophobic domain (HD): light blue; sequences for ATP binding (Walker A) and ATP hydrolysis (Walker B, Sensor 1, 2): dark blue [36-39]; positions of p.Ser112Arg and p.Arg288* variants: red; supposed deletion of C-terminal amino acids due to the p.Arg288* nonsense variant: red hatched.

(B) Structural model of torsinA (Protein Data Bank accession code: 5J1S)

β -sheets: light green; α -helices: dark green; loops: grey; p.Ser112Arg and p.Arg288* variants and supposed C-terminal deleted regions due to the p.Arg288* variant: red; sequences for ATP binding (Walker A) and ATP hydrolysis (Walker B, Sensor 1, 2): dark blue [36-39]. The image was created using PyMOL, version 1.8.2.0 (Schrödinger, LLC).

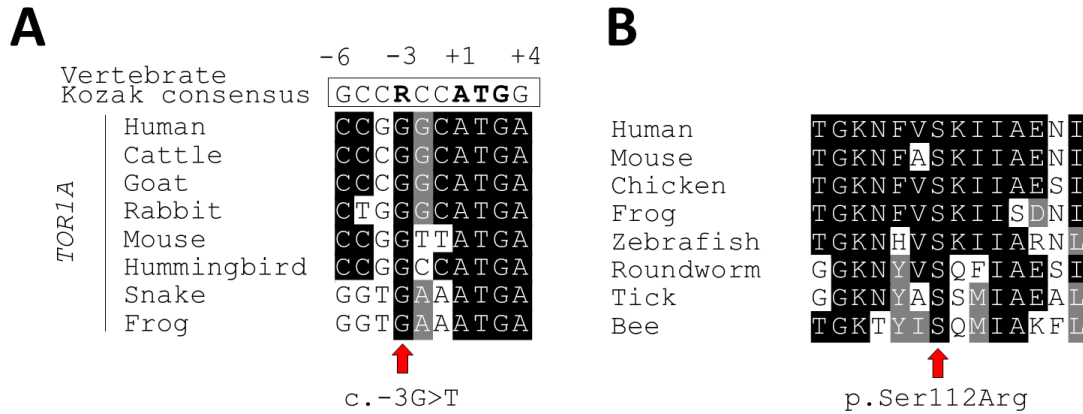


Figure 4: Multiple Sequence Alignments (MSA) for p.Ser112Arg and c.-3G>T variants

(A) MSA of *TOR1A* Kozak sequences from different vertebrate species

A red arrow marks the position of variant c.-3G>T. The vertebrate Kozak consensus sequence [109] is depicted above the sequence alignments. R represents a random purine base (A or G). The following DNA sequences were used: Human (*H. sapiens*): NM_000113.3, cattle (*B. taurus*): NM_001099058.2, goat (*O. aries*): XM_004007147.3, rabbit (*O. cuniculus*): XM_008251716.2, mouse (*M. musculus*): NM_144884.2, hummingbird (*C. anna*): XM_008491452.2, snake (*P. textilis*): XM_026712241.1, frog (*N. parkeri*): XM_018558540.1.

(B) MSA of torsinA amino acid sequences around residue p.Ser112 in vertebrates and non-vertebrates

A red arrow marks the position of variant p.Ser112Arg. The following protein sequences were used: Human (*H. sapiens*): NP_000104.1, mouse (*M. musculus*): NP_659133.1, chicken (*G. gallus*): NP_001025858.1, frog (*X. tropicalis*): NP_001039096.1, zebrafish (*D. rerio*): NP_957150.1, roundworm (*T. spiralis*): XP_003379108.1, tick (*R. appendiculatus*): JAP82267.1, bee (*A. cerana cerana*): PBC30553.1.

5.4 Clinical presentation of *TOR1A* related AMC

Family A is a non-consanguineous Kosovar family with healthy parents and two affected boys (A-II:1 and A-II:2) who carry the homozygous p.Arg288* *TOR1A* variant (Figure 5). There was no history of neurological disease in the parents and the wider family. Both pregnancies were complicated by polyhydramnios and both boys were born via caesarian section because of fetal hypokinesia (A-II:2) and birth arrest (A-II:1). Both neonates showed insufficient adaptation to extrauterine life, respiratory distress with labored, gasping breathing as well as retrognathia, multiple contractures in all extremities, inguinal herniation and bilateral hip dysplasia (Figure 6). Neurological examination revealed generalized muscle hypertonicity, poor spontaneous movements and bulbar dysfunction. Myoclonic jerks were observed in one child (A-II:2). Both boys died of respiratory failure at the age of 4 (A-II:1) and 11 weeks (A-II:2).

Electroencephalography (EEG), electromyography (EMG), nerve conduction studies, measurement of serum creatine kinase (CK) levels, metabolic screening and skeletal muscle biopsy histology (A-II:2) did not contribute to identify the cause of the patients' condition. Screening for maternal myasthenia gravis, *SMNI*, *RAPSN* and *CHRNA3* mutation analysis as well as karyotyping were all unremarkable. Brain MRI of patient A-II:2 revealed hypomyelination of the optical tract, motor cortex and corticospinal tract (Table S3, Table S4, Table S5).

Family B is a Kosovar family not knowingly related to family A. The healthy, non-consanguineous parents had two affected sons (B-II:1 and B-II:2) carrying the same homozygous p.Arg288* *TOR1A* variant that was identified in family A (Figure 5). Family history was unremarkable for neurological diseases. Both children showed reduced fetal movement during pregnancy. Both neonates presented with insufficient adaptation to extrauterine life, respiratory distress, retrognathia, multiple contractures and inguinal herniation. Neurological examination revealed bulbar dysfunction, generalized muscle weakness and involuntary myoclonus-like trembling movements. Both infants died of respiratory failure at the age of 4 (B-II:1) and 5 weeks (B-II:2). EEG, EMG, nerve conduction studies, measurement of serum CK levels, metabolic screening, cerebrospinal fluid analysis and muscle biopsy histology (B-II:1) did not reveal pathological findings. Molecular karyotyping by array-based comparative genomic hybridization was also unremarkable. Brain MRI (B-II:1) displayed widening of subependymal spaces and occipital horns together with hypomyelination of occipital subcortical white matter (Table S3, Table S4, Table S5).

Parents of Family C were of Spanish origin, non-consanguineous and reportedly healthy. The couple had a single affected child (C-II:1) carrying the compound heterozygous c.-3G>T, p.Ser112Arg and c.339G>A variants (Figure 5). At birth, the boy presented with poor spontaneous movements, multiple contractures in all extremities, opisthotonos and umbilical herniation (Figure 6). He was initially tube-fed because of poor suck and improper swallowing; however, symptoms improved within the first week of life and completely resolved later. Respiratory function was unaffected. Dystonia-like hand movements were reported during the first 6 months of life but ceased afterwards. Contractures improved over time, but generalized weakness and increased muscle tone persisted. All motor milestones were delayed and he did not start to walk with support until the age of 3 years. When last seen at the age of 8 years, he could get up from the floor with "Gowers maneuver", walked without assistance with a spastic gait and needed support when

climbing stairs. Speech was dysarthric, he had partial neurosensory deafness and verbal expression and comprehension were limited. Brain MRI, EEG, EMG, nerve conduction studies and *CHRNA3* mutation analysis were unremarkable (Table S3, Table S4, Table S5).

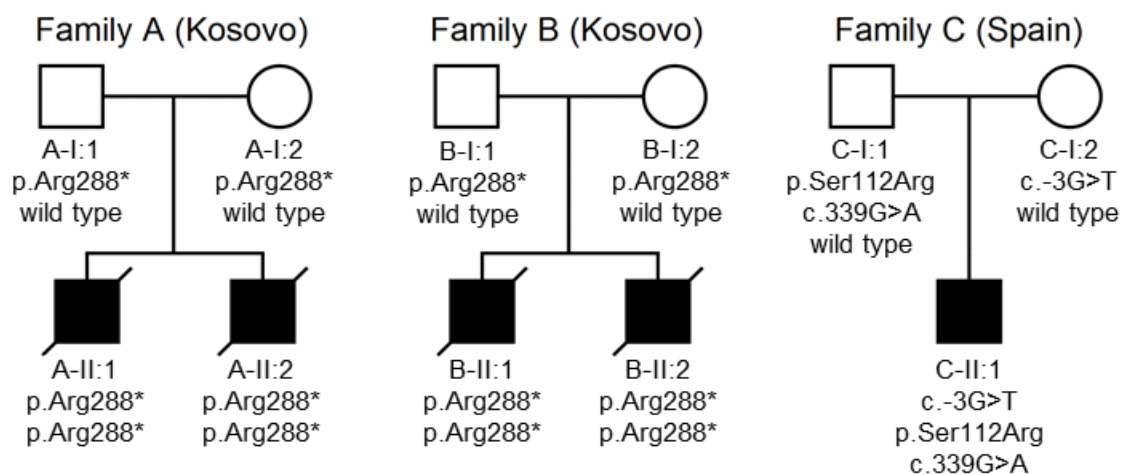


Figure 5: Pedigrees of families A, B and C

Squares represent males, circles represent females and filled symbols represent affected family members. Symbols with a diagonal line indicate deceased individuals.



Figure 6: Clinical photographs of individuals with biallelic *TOR1A* variants

Left panel: images of patients A-II:1 and A-II:2 with severe AMC. Note retrognathia, elbow flexion contractures, clenched fingers and rocker-bottom like feet.

Right panel: images of patient C-II:1 with milder form of AMC. Note clenched fingers and toes, multiple contractures in other joints and large umbilical hernia (at ages 1 and 4 months (mo.)). Contractures largely improved with age and he gained proper hand use (at age 3 years (yr.)). At the age of 8 years, contractures were barely noticeable anymore.

5.5 Levels of overexpressed wild-type and mutant torsinA in HEK293 cells

To evaluate possible consequences of *TOR1A* variants on the availability of torsinA in cells, we initially attempted to determine torsinA levels by western blotting in patient-derived primary skin fibroblasts compared to non-disease control cells. Unfortunately, the antibody we used (clone D-M2A8) produced unspecific signals similar to the predicted size of truncated p.Arg288* torsinA, obscuring proper detection and quantification of mutant protein (Figure S1, Figure S2). Therefore, we decided to make use of overexpression experiments with epitope-tagged torsinA and subsequent convenient detection with an antibody recognizing the epitope tag. Wild-type (wt), p.Arg288* and p.Ser112Arg mutant *TOR1A* cDNA sequences were C-terminally fused to GFP and transiently transfected into HEK293 cells. Following cell lysis and protein extraction, western blot analysis using an anti-GFP antibody revealed significantly decreased levels of mutant torsinA compared to wild-type protein (Figure 7). The levels of p.Arg288*-torsinA-GFP was decreased to around 20 % of the wild-type signal, while the p.Ser112Arg variant yielded torsinA levels corresponding to around 40 % of the wild-type protein.

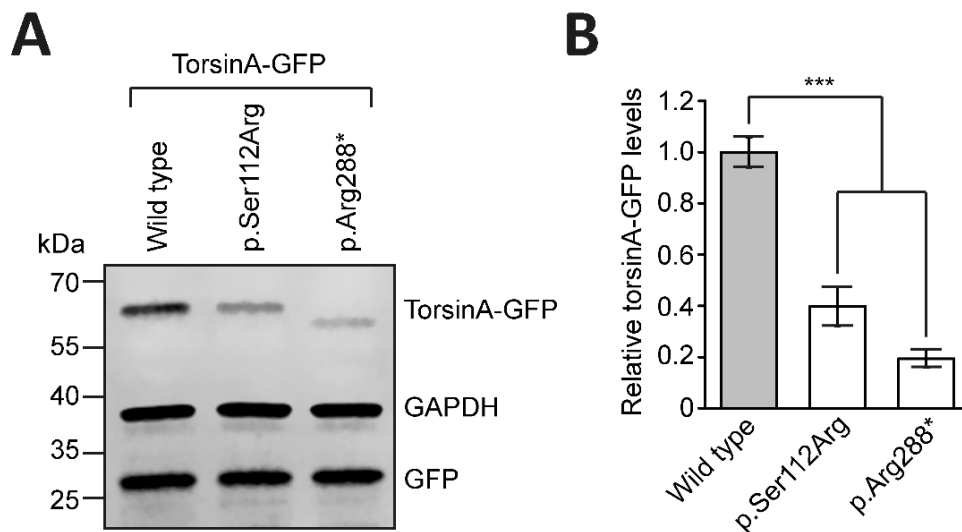


Figure 7: Levels of p.Ser112Arg and p.Arg288* torsinA-GFP in HEK293 cells

(A) Representative western blot for overexpressed wild type and mutant torsinA-GFP

HEK293 cells were transiently co-transfected with indicated *TOR1A*-GFP constructs and empty GFP expression vector (transfection efficiency control). An anti-GFP antibody was used to detect torsinA-GFP constructs and GFP. Endogenous levels of GAPDH were used as loading control.

(B) Quantification of torsinA-GFP levels

TorsinA-GFP levels were quantified and normalized to GFP and GAPDH signals. The diagram shows means and standard deviations of n=3 independent experiments. *** indicates P<.001 (two-tailed Student's t-test).

5.6 Degradation kinetics of wild-type and mutant torsinA

Having established that torsinA variants p.Arg288* and p.Ser112Arg were associated with reduced torsinA abundance, we next attempted to discriminate the relative effects of translation and proteolysis on levels of mutant torsinA. In order to specifically analyze protein degradation, we performed cycloheximide chase followed by western blotting. In this procedure, aliquots of cells are collected at specific time points following addition of the translation inhibitor cycloheximide [113, 114]. Because protein synthesis is blocked, changes in protein abundance can be attributed to protein degradation.

TOR1A-GFP expression constructs were transfected into HEK293 cells and the proportion of torsinA protein remaining at several time points was quantified. The abundance of wild-type torsinA remained relatively constant during the course of the experiment, similar to levels of GFP (co-transfected as a control for similar transfection efficiency) and a loading control protein (GAPDH). p.Ser112Arg and p.Arg288* torsinA-GFP were more rapidly degraded than the wild-type protein (Figure 8). After 4 hours, abundance of p.Arg288* torsinA was reduced to less than 40 % of the initial levels, while p.Ser112Arg torsinA showed a less dramatic decrease of abundance to about 70 % of the initial levels.

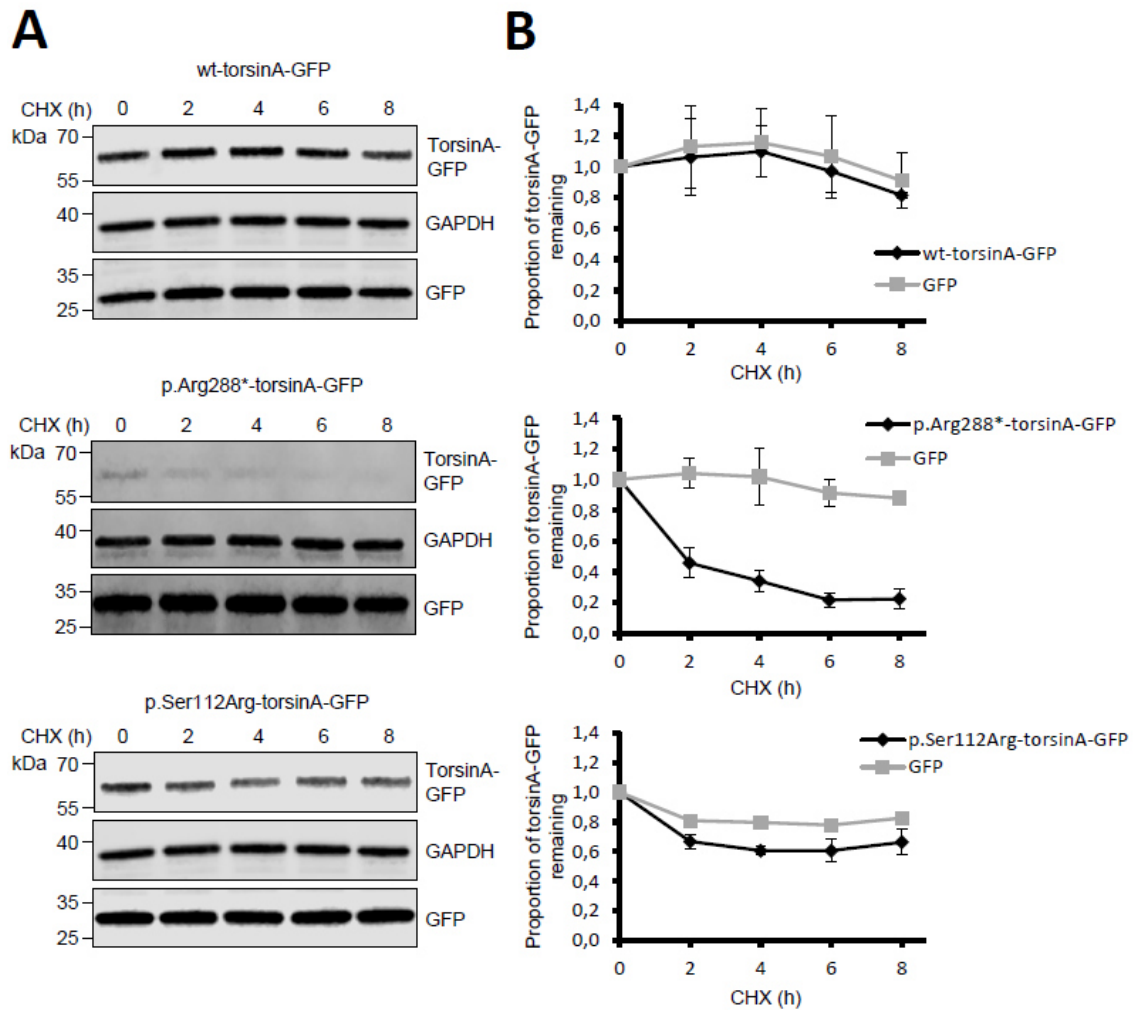


Figure 8: Cycloheximide chase followed by western blotting

(A) Representative western blot results for wild-type, p.Arg288*- and p.Ser112Arg-torsinA-GFP

HEK293 cells were transiently co-transfected with *TOR1A*-GFP constructs and empty GFP expression vectors (transfection efficiency control). Cells were treated 24 h post-transfection with 20 $\mu\text{g/ml}$ cycloheximide (CHX) and harvested 2, 4, 6 and 8 h after treatment. An anti-GFP antibody was used to detect torsinA-GFP constructs and GFP empty vector control. Endogenous levels of GAPDH were used as loading control.

(B) Quantification of torsinA-GFP and GFP levels

TorsinA-GFP and GFP levels were quantified and normalized to GAPDH levels and plotted for each time point. Graphs represent means and standard deviations of n=3 experiments.

5.7 Degradation of wild-type and mutant torsinA through proteasome and autophagy pathways

Results of the cycloheximide chase assay suggested that mutant torsinA was rapidly degraded in cells. Previous publications reported that both proteasome activity and autophagy are involved in torsinA degradation [16, 115, 116]. Therefore, HEK293 cells

transiently transfected with wild-type or mutant *TOR1A* expression constructs were either treated with MG132 to inhibit the proteasome pathway or with bafilomycin A1 to block autophagic flux.

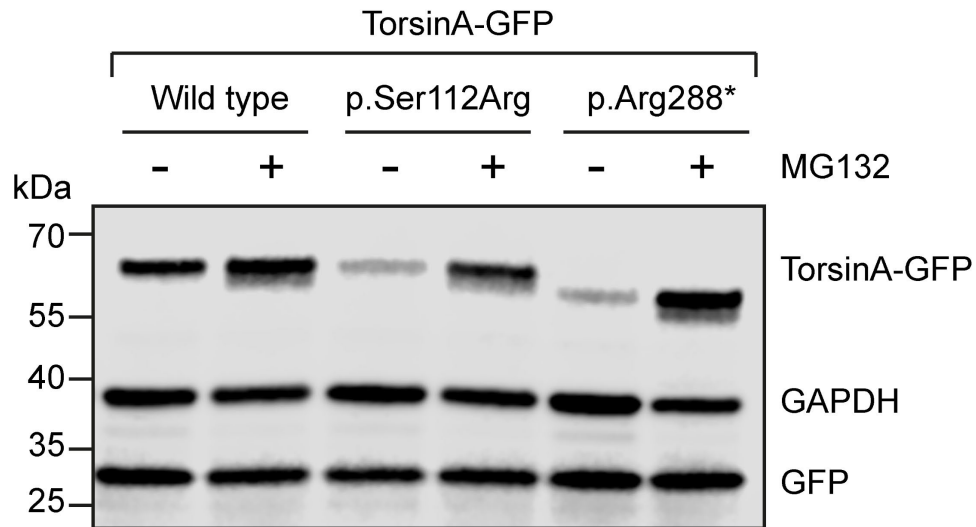


Figure 9: Effect of proteasome inhibition on torsinA-GFP levels

Representative results of MG132 treatment of HEK293 cells transiently co-transfected with *TOR1A*-GFP constructs and empty GFP expression vector (transfection efficiency control). Seven hours post transfection cells were treated with 5 μ M MG132 (+) or DMSO as a vehicle control (-) for 17 h. An anti-GFP antibody was used to detect torsinA-GFP constructs and GFP empty vector control. Endogenous levels of GAPDH were analyzed to control for equal loading of total cellular protein.

MG132 treatment led to a strong increase of abundance of p.Arg288*- and p.Ser112Arg-torsinA-GFP, resulting in protein levels comparable to overexpressed wild-type protein (Figure 9). Conversely, bafilomycin A1 treatment had neither an effect on protein levels of the p.Arg288* and p.Ser112Arg variants nor on wt-torsinA-GFP (Figure 10). Efficient blockade of autophagic flux was confirmed by increase of autophagy marker LC3-II.

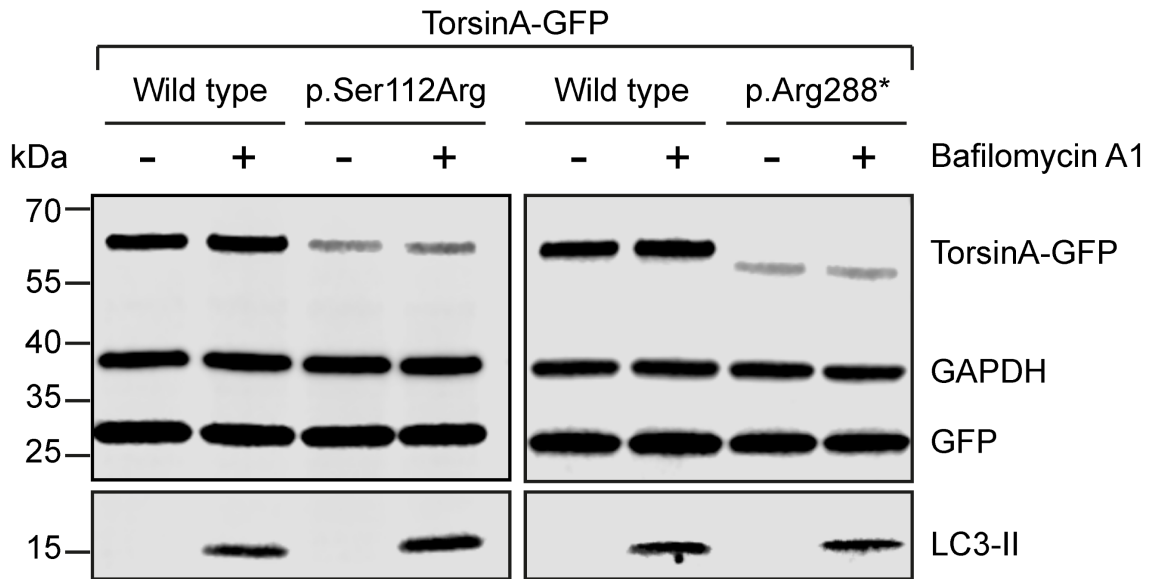


Figure 10: Effect of autophagy inhibition on torsinA-GFP levels

Representative results of bafilomycin A1 treatment of HEK293 cells transiently co-transfected with *TOR1A*-GFP constructs and empty GFP expression vector (transfection efficiency control). Twelve hours post transfection cells were treated with 0.1 μ M bafilomycin A1 (+) or DMSO as a vehicle control (-) for 12 h. An anti-GFP antibody was used to detect torsinA-GFP constructs and GFP empty vector control. Endogenous levels of GAPDH were analyzed to control for equal loading of total cellular protein. LC3-II was used as marker to ensure successful inhibition of autophagy.

5.8 Effect of *TOR1A* variants on torsinA's subcellular localization

Immunofluorescence microscopy was performed to examine whether the *TOR1A* variants altered torsinA's subcellular localization. HeLa cells were transiently transfected with expression constructs for AMC-related p.Ser112Arg and p.Arg288* torsinA-GFP mutants, wild-type torsinA-GFP or an artificial ATP-trap-mutant (p.Glu171Gln), which has been reported to accumulate in the nuclear envelope [32]. Wild-type torsinA-GFP showed a regular localization throughout the endoplasmic reticulum and nuclear envelope as described in the literature [31, 32]; however, p.Ser112Arg-torsinA-GFP accumulated in the nuclear envelope, similar to the ATP-trap-mutant p.Glu171Gln. Consistent with low levels documented by western blotting analysis, the p.Arg288* variant gave a very faint signal, but no obvious change of its subcellular localization was observed (Figure 11).

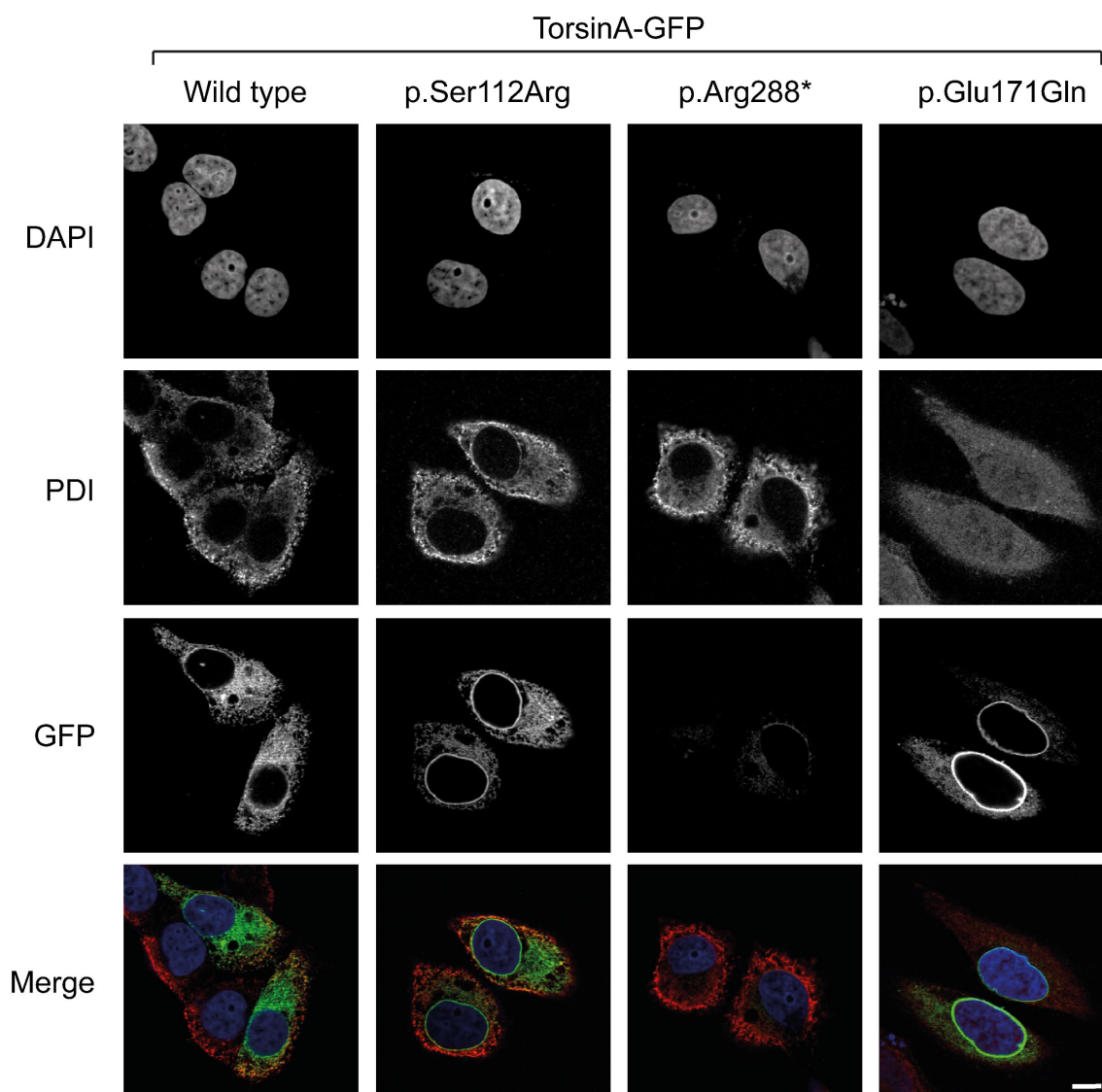


Figure 11: Immunofluorescence staining of HeLa cells transiently transfected with *TOR1A*-GFP constructs

HeLa cells were transiently transfected with *TOR1A*-GFP constructs, including wt, p.Arg288*, p.Ser112Arg and p.Glu171Gln *TOR1A* variants. Cells were stained with anti-PDI antibody (red) for endoplasmic reticulum labelling and with DAPI (blue) for nuclei. TorsinA species were visualized through recording of the GFP signal. Scale bar, 10 μ m.

5.9 TorsinA levels associated with the *TOR1A* c.-3G>T variant

In order to analyze the effect of the c.-3G>T Kozak sequence variant on torsinA levels, the 5'-UTR sequence of the pEGFP-N1 vector containing the *TOR1A* open reading frame was replaced by a partial *TOR1A* 5'-UTR sequence with or without the c.-3G>T substitution (Figure 12, A). Following overexpression in HEK293 cells, western blotting revealed a significant reduction of torsinA-GFP levels when the Kozak sequence contained the c.-3G>T variant (Figure 12, B, C).

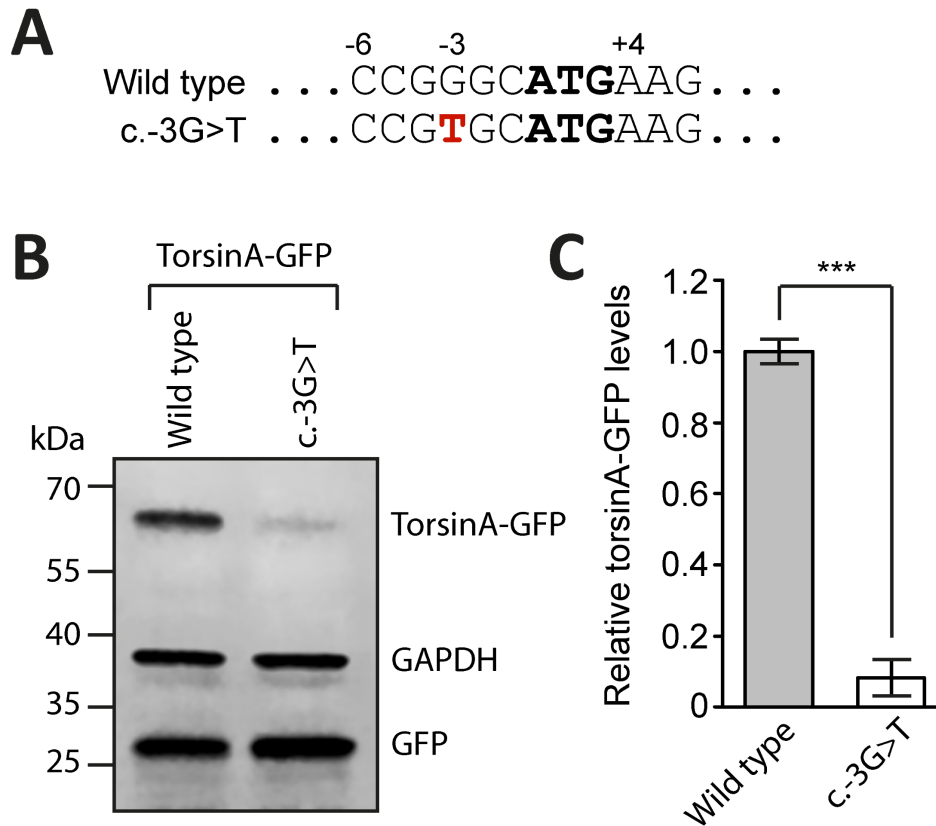


Figure 12: Western blot analysis of the c.-3G>T *TOR1A* variant

(A) Kozak sequence of human wild-type and c.-3G>T mutated *TOR1A*

Positions -6 and +4 correspond to the borders of the Kozak sequence [109]. The c.-3G>T variant is highlighted in red.

(B) Representative western blot

HEK293 cells were transiently transfected with GFP expression vectors containing the *TOR1A* ORF preceded by wild-type or c.-3G>T *TOR1A* 5'-UTR. An empty GFP vector was co-transfected to control for equal transfection efficiency. An anti-GFP antibody was used to detect torsinA-GFP constructs and GFP empty vector. Endogenous levels of GAPDH were used as loading control.

(C) Quantification of torsinA-GFP levels

TorsinA-GFP levels were quantified and normalized to GFP levels. The diagram represents means and standard deviations of n=3 experiments. *** indicates P<.001 (two-tailed Student's t-test).

5.10 Translational activity of the *TOR1A* c.-3G>T cDNA

To assess translational activity of the c.-3G>T variant, a reporter gene was constructed consisting of the wild-type or c.-3G>T *TOR1A* Kozak motif followed by the firefly luciferase cassette of the pGL4.26 vector (Figure 13, A). The *TOR1A* wild-type Kozak sequence led to a modest decrease of firefly luciferase luminescence compared to the native pGL4.26 Kozak sequence, which is most likely explained by the incomplete Kozak consensus sequence of *TOR1A* opposed to the optimized Kozak motif of the vector.

Conversely, the substitution of guanine with thymine at position -3 of the *TOR1A* 5'-UTR led to a significant reduction of firefly luciferase luminescence to about 50 % of the wild-type signal (Figure 13, B).

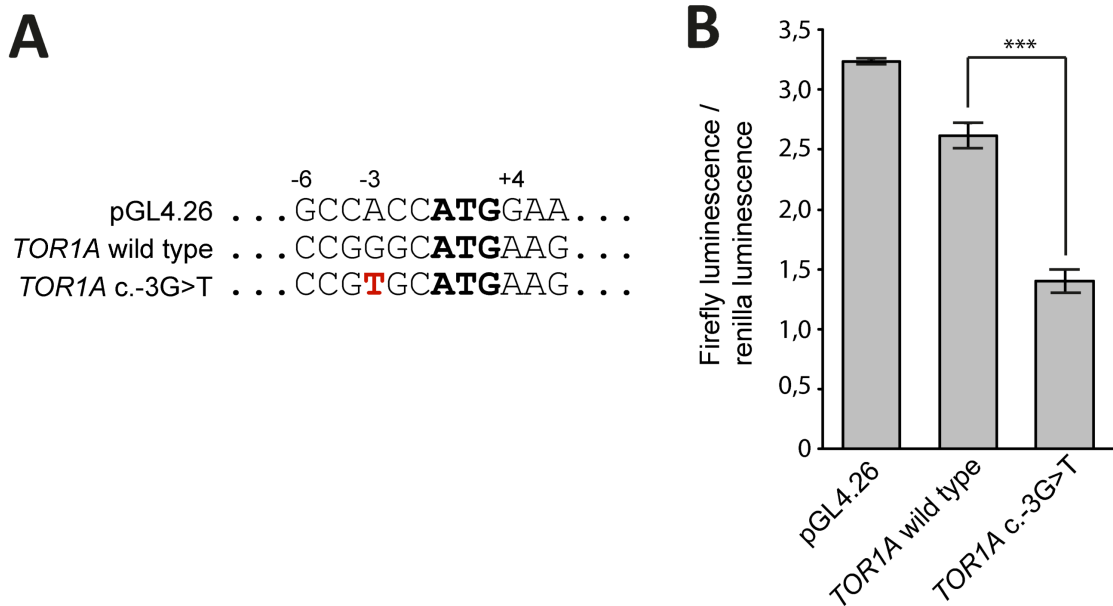


Figure 13: Dual luciferase reporter assay of the c.-3G>T variant

(A) Kozak sequences of pGL4.26 vector, wild-type *TOR1A* and the *TOR1A* c.-3G>T variant
Positions -6 and +4 constitute the borders of the Kozak sequence [109]. The c.-3G>T variant is highlighted in red.

(B) Results of the dual luciferase reporter assay

HEK293 cells were transiently transfected with pGL4.26 vectors containing pGL4.26 standard, *TOR1A* wild-type or *TOR1A* c.-3G>T 5'-UTR sequences. A pRL-TK (Renilla luciferase) vector was co-transfected. Firefly and Renilla luminescence were measured and the ratio was calculated. The diagram shows means and standard deviations of n=4 experiments. *** indicates P<.001 (two-tailed Student's t-test).

5.11 Effect of *TOR1A* variants on LAP1 and LULL1 localization

In order to test if the *TOR1A* variants had an effect on the localization of torsinA binding partners LAP1 or LULL1, C-terminally HA-tagged LAP1 and LULL1 were overexpressed in primary skin fibroblasts obtained from patients with the homozygous p.Arg288* and compound heterozygous c.-3G>T and p.Ser112Arg *TOR1A* variants and a non-disease control sample. Irrespective of the *TOR1A* genotype, detection of LAP1-HA and LULL1-HA by immunofluorescence staining with an anti-HA antibody revealed that LAP1-HA was present in the NE while LULL1-HA was detected in both the ER and

NE (Figure 14). This pattern represented the known natural localizations of LAP1 and LULL1 [43].

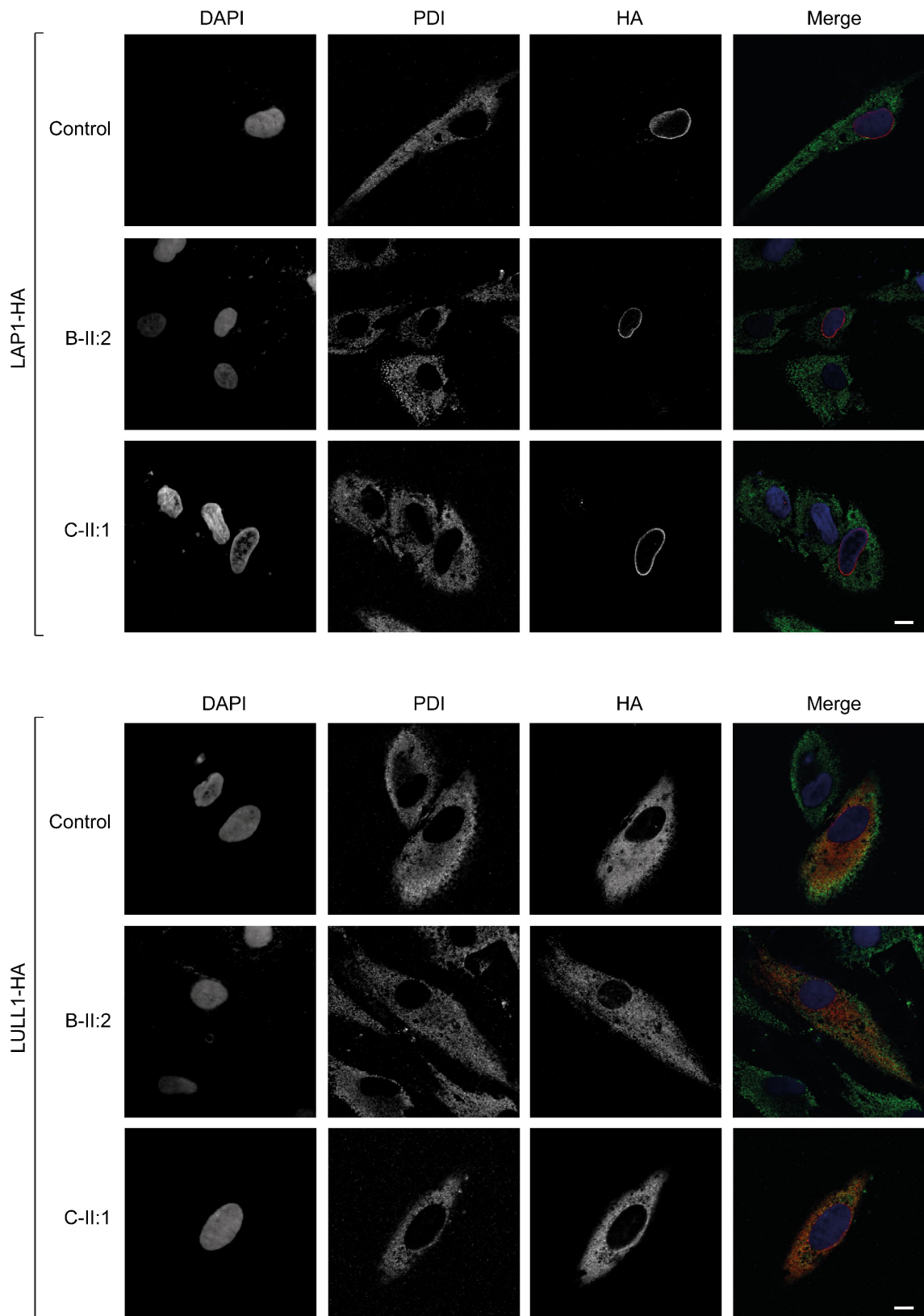


Figure 14: Immunofluorescence staining of primary skin fibroblasts transiently transfected with LAP1- and LULL1-HA constructs

Patients' (B-II:2 and C-II:1) and control primary human dermal fibroblasts were transiently transfected with C-terminal HA tagged LAP1 (upper panel) and LULL1 (lower panel) constructs. Cells were stained with anti-HA (red) and anti-PDI (green, ER) antibodies and with DAPI (blue, nuclei). Scale bar, 10 μ m.

5.12 Effects of TOR1A variants on nuclear movement in polarizing cells

Several recent studies suggest that torsinA is required for centrosome orientation and rearward nuclear movement in migrating fibroblasts [63, 64]. To examine centrosome reorientation in control and patient-derived fibroblasts, cells were grown in a confluent monolayer, scratched with a pipette tip and stimulated by LPA. Positioning of the centrosomes in cells bordering the scratch wound was examined by immunofluorescence microscopy (Figure 15). Fibroblasts carrying the homozygous p.Arg288* variant (patient B-II:2) showed a significant decrease in centrosome reorientation compared to a non-disease control; however, in fibroblasts of patient C-II:1 carrying the compound heterozygous variants c.-3G>T and p.Ser112Arg, no significant change in centrosome reorientation was detectable.

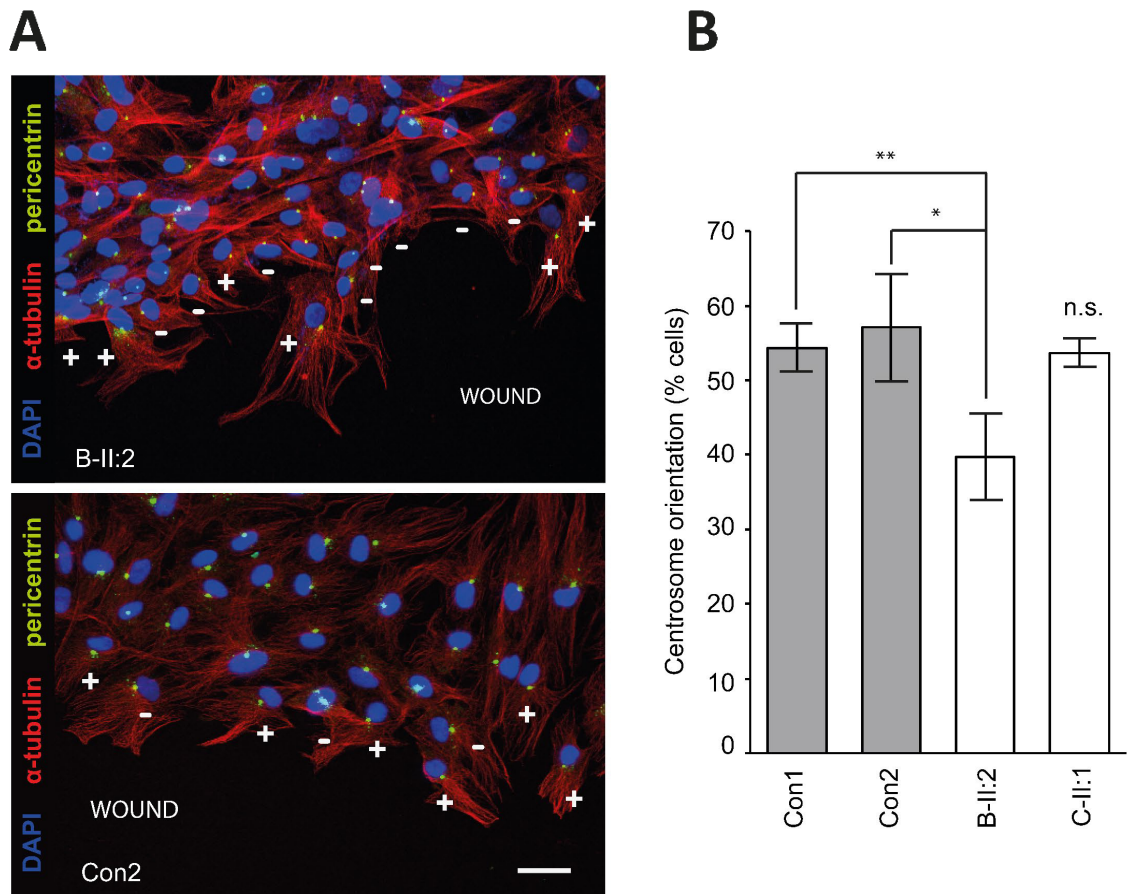


Figure 15: Centrosome reorientation in polarizing patient and control fibroblasts

Patient (B-II:2 and C-II:1) and control (Con1, Con2) human primary dermal fibroblasts were grown until confluency. After serum withdrawal for 24 h, the monolayer was scratched using a pipette tip and cells were cultured another 3 h in culture medium containing 2 μ M LPA.

(A) Representative immunofluorescence pictures

Immunofluorescence staining was performed using anti-pericentrin (green, centrosomes) and anti- α -tubulin (red, microtubules) antibodies and DAPI (blue, nuclei). Centrosomes in cells bordering the scratch wound were considered as correctly orientated (+) if they were located between the nucleus and the leading edge of the cell. Otherwise centrosomes were classified as incorrectly orientated (-) [105]. Scale bar, 40 μ m.

(B) Quantification of centrosome reorientation

At least 100 cells were counted per condition and the percentage of cells with correctly orientated centrosomes was calculated. The diagram shows means and standard deviations of $n=3$ experiments. * denotes $P<0.05$ and ** denotes $P<0.01$ (two-tailed Student's t-test). n.s.: not significant.

5.13 Effects of *TOR1A* variants on fibroblast migration

Several recent studies suggested that torsinA is also required for efficient fibroblast migration [55]. Therefore, the migration ability of patients' fibroblasts was examined in a standardized wound healing assay using IBIDI culture inserts that allowed generation of a reproducible gap in the culture monolayer. The fibroblasts of patient B-II:2 carrying the

homozygous p.Arg288* variant showed delayed closure of the gap: While control fibroblasts had invaded the gap and covered most of the defect after 24 h, the gap in the B-II:2 fibroblast culture was still clearly demarcated, and only few cells had reached the midline of the gap. After 48 h the gap was completely covered by control fibroblasts but not by p.Arg288* mutant cells. In contrast, fibroblasts of patient C-II:1, carrying the compound heterozygous variants c.-3G>T and p.Ser112Arg, were indistinguishable from non-disease control cells (Figure 16).

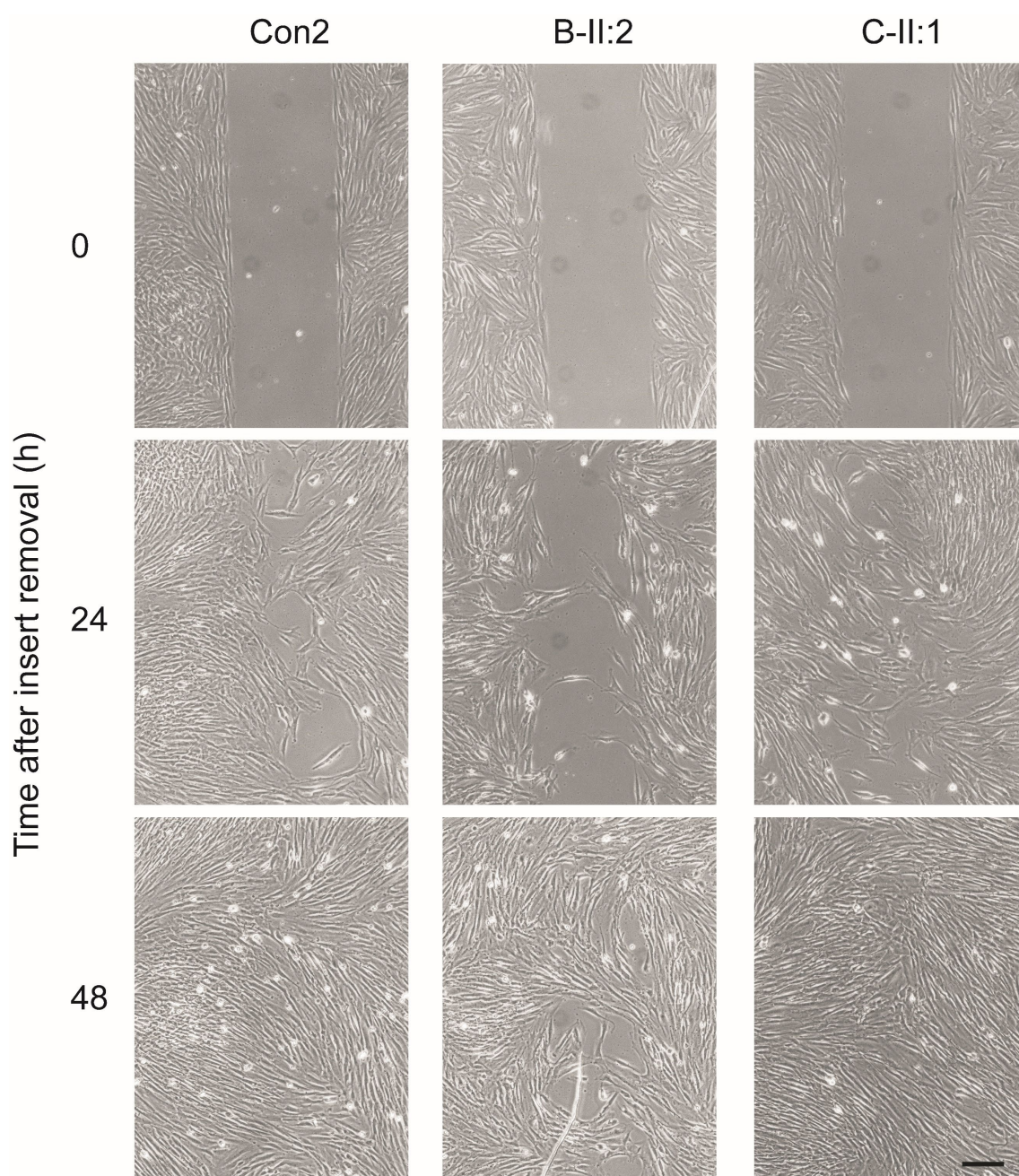


Figure 16: Wound healing assay using patients' dermal fibroblasts

Patient (B-II:2 and C-II:1) and control (Con2) primary human dermal fibroblasts were cultured until confluency in IBIDI 35 mm μ -Dishes with 2 well culture inserts. At confluency level inserts

were taken out leaving a gap of 500 μm in the monolayer. Pictures of the gap were taken every 24 h to monitor migration of cells. The experiment was repeated three times with similar results. Scale bar 200 μm .

.

6 Discussion

Heterozygous variants in the *TOR1A* gene are a long-recognized cause of autosomal dominantly inherited torsion dystonia (DYT1) [3, 15-19]. More recently, bi-allelic *TOR1A* variants were identified in children with a different clinical presentation, autosomal recessive arthrogryposis multiplex congenita (AMC) [27, 28, 106]. This study reports on further patients with *TOR1A*-related AMC, extends the clinical and mutational spectrum and provides experimental evidence supporting pathogenicity of these *TOR1A* variants.

Previous reports indicated that *TOR1A*-related AMC is a severe form of AMC, usually complicated by massive global developmental delays and - in most severely affected individuals - respiratory compromise and death during infancy [27, 28, 106]. In this study, all four patients with the p.Arg288* variant presented with this severe extreme of the phenotype, confirming one previous case study of a patient with this particular variant [28]. They all showed generalized contractures at birth, insufficient adaptation to extrauterine life, neonatal respiratory distress, massive global developmental delays and death within the first months of life. Other patients with different genotypes had milder disease without respiratory compromise and early fatality; however, they all presented with multiple contractures that seemed to improve over time, could not ambulate and had severe global developmental delays [106]. The individual with the compound heterozygous c.-3G>T and p.Ser112Arg variants identified in this study seems to represent an even milder form of *TOR1A*-related AMC with nearly complete relief of contractures over time and slow but steady motor development. He also had possible mild to moderate mental retardation; however, no formal testing was performed to confirm this clinically suspected diagnosis and cognitive capacities were also difficult to assess because of partial deafness and dysarthric speech.

All *TOR1A* variants identified in this study were shown to lead to reduced levels of torsinA, though to a variable degree. Differences in amounts of remaining torsinA may correlate with severity of the phenotype: The homozygous p.Arg288* variant - associated with severe disease - resulted in barely detectable amounts of torsinA while compound heterozygous variants c.-3G>T and p.Ser112Arg - associated with much milder clinical presentation - were related to less drastically reduced amounts of remaining torsinA protein. Although low torsinA levels seem to constitute a net consequence of *TOR1A* variants investigated in this study, depletion of torsinA is most likely caused by different variant-specific mechanisms: The c.-3G>T variant changes one of the most invariant positions in

the eukaryote translation initiation site [110, 111, 117] and was experimentally found to interfere with efficient translation of *TOR1A* mRNA. Conversely, the rate of synthesis of p.Arg288* and p.Ser112Arg variants is probably similar to the wild-type protein; however, mutant torsinA species appear to be prone to rapid proteasomal degradation. Beside its effect on torsinA levels, missense variant p.Ser112Arg also altered subcellular localization of torsinA, shifting it predominantly to the NE. A similar recruitment to the NE was previously reported for other *TOR1A* variants, including AMC-related p.Glu303del and p.Gly318Ser as well as ATP hydrolysis deficient Walker A, B, sensor 1 and 2 variants [32, 106, 118]. Concerning the truncating variant p.Arg288*, it was additionally predicted to have lost its ATPase activity as critical protein regions are missing due to early termination of translation (although the biological relevance of this observation is unclear as only minute amounts of p.Arg288* torsinA are present in cells). Altogether, this data suggests decreased availability of functional torsinA at its site of normal biological activity, consistent with a loss-of-function mechanism which is in general agreement with autosomal recessive transmission of *TOR1A*-related AMC [27, 28, 106].

Current concepts of DYT1 pathophysiology are based on the idea that *TOR1A* variants, including the common p.Glu303del variant, represent loss-of-function alleles that result in haploinsufficiency [44, 65], although some earlier studies had attributed gain of (toxic) function effects to DYT1 variants [31, 119]. A loss-of-function mechanism is further supported by the observation that the common p.Glu303del DYT1 variant has been identified in cases with AMC as well [27, 106]. Based on these findings, it was unexpected that none of the obligate heterozygotes in AMC families in this and previous studies had overt symptoms or signs of torsion dystonia [27, 28, 106]. To date, the most plausible explanation is incomplete penetrance in carriers of heterozygous variants. Notably, penetrance of the best studied heterozygous *TOR1A* variant, p.Glu303del, was estimated to be as low as 30-40 % and it seems reasonable to assume that other *TOR1A* alleles behave in a similar way [4].

The identification of *TOR1A* variants as the cause of DYT1 torsion dystonia in 1997 has sparked intense research into torsinA biology and its relation to disease [3]. Many different molecular and cellular functions have been assigned to torsinA [66, 67, 75, 77, 120]; however, it is still unclear which of these mechanisms are related to the pathophysiology of torsinA-associated diseases. Consistent with findings in torsinA depleted cells [55, 64], drastically reduced torsinA levels in p.Arg288* fibroblasts were associated with abnormal centrosome orientation, nuclear positioning and migration abilities. Conversely, no

such abnormalities were seen in fibroblasts with variants c.-3G>T and p.Ser112Arg and less drastically reduced torsinA levels. On the one hand, these inconsistent findings may argue against a relevant contribution of abnormal centrosome orientation and nuclear positioning to the pathogenesis of torsinA-related AMC. On the other hand, similar to the potential relationship between remaining torsinA levels and clinical outcome, a “gene dose effect” may account for this observation: Impairment of centrosome orientation and nuclear positioning might be less obvious in cells with less severely diminished torsinA content and may therefore escape detection by the assays used in this study.

AMC can be caused by central nervous system dysfunction or arise from alterations in the periphery, for example disturbed function of skeletal muscle, neuromuscular junction or peripheral nerves [24, 26]. Normal muscle biopsy histology, CK levels, EMG and ENG findings as opposed to subtle brain MRI changes of the described cases support abnormal central nervous system (CNS) function as pathophysiologic origin of *TOR1A*-related AMC, also consistent with the role of torsinA in a movement disorder like DYT1 torsion dystonia [65]. Of note, mice with homozygous conditional *Tor1A* knockout in CNS neurons had a phenotype reminiscent of severe AMC, including abnormal posturing of extremities, failure to thrive and early lethality [65, 121]; however, the possible connection with AMC was not discussed in the study, which put focus on dystonia and was published before the discovery of biallelic *TOR1A* variants in individuals with AMC [121]. Furthermore, abnormal brain morphology was reported in embryonal and postnatal brains of homozygous conditional *Tor1A* knockout mice, supporting the hypothesis that *TOR1A*-related AMC is caused by CNS dysfunction [120, 121].

TOR1A is ubiquitously expressed; however, lack of torsinA seems to affect predominantly the CNS [65]. One explanation for this discrepancy might be that the closest torsinA homologue, torsinB, shows low levels in the CNS at early stages of CNS development while being broadly expressed in other tissues [122-124]. TorsinB may thus compensate for the reduction or loss of torsinA in peripheral tissues. Of note, the NE-“blebbing” phenotype of torsinA deficient neurons can be reproduced in non-neuronal cell populations by simultaneous knock-out of both, torsinA and B [65, 125, 126].

Moreover, torsinB overexpression in conditional neuronal *Tor1A* knockout mice led to amelioration of abnormal postures, weight loss and early lethality [126, 127]. Under physiological conditions, torsinB levels increase in maturing neurons at later stages of CNS development [124]. This increase could explain the later amelioration of the phenotype in those individuals with *TOR1A*-related AMC who survive beyond the first months of

life [123, 124]. Consistent with this hypothesis, a recent study showed improvement of contractures in conditional neuronal *Tor1A* knockout mice when surviving beyond the lactation period [128]. Summing up these findings, early upregulation of torsinB in the developing CNS might constitute a potential therapeutic option for *TOR1A*-related AMC.

The present study is hoped to improve the current understanding of *TOR1A*-related pathologies and may help to resolve some of the uncertainties discussed above. Nevertheless, it has several obvious limitations. First, due to issues with the specificity of the anti-torsinA antibody and inaccessibility of affected neural tissue, we were unable to study endogenous levels of mutant torsinA in relevant cell types. On the other hand, overexpression studies in transfected cells represent an established technique for testing effects of mutants and can provide a reasonable approximation of the true effects of variants. Second, we did not directly investigate ATPase activity of torsinA which would be important to completely evaluate functional consequences of *TOR1A* variants. On the other hand, low levels and aberrant localization of mutant torsinA are expected to reduce availability of functional torsinA at its sites of action, even if the activity had been unchanged. Third, we did not study the silent variant c.339G>A *in trans* with the p.Ser112Arg missense variant further. In theory, this variant may affect pre-mRNA splicing, alter mRNA stability or impair translation [129-131]; and all these potential consequences are predicted to lead to a reduction of torsinA levels. As c.339G>A would have an effect, if any, in the same direction as other AMC-related *TOR1A* variants had, further studies on this variant are unlikely to challenge results and interpretation of experiments presented here. Finally, based only on few cases reported here and elsewhere, it is too premature to establish a firm correlation between remaining levels of torsinA and disease severity. Although our data suggest such a correlation, further studies involving more carefully phenotyped individuals with *TOR1A*-related AMC together with thorough evaluation of torsinA protein levels associated with the respective variants will be needed to substantiate this hypothesis.

7 Supplemental material

7.1 Whole exome sequencing output

Table S1: Whole exome sequencing output

Sequenced family	Family A
Enrichment	Agilent SureSelect50Mbv5
Sequencing type	Affected proband WES
Platform	Illumina HiSeq2000
Read alignment	BWA (v0.5.8)
Variant calling	SAMtools (v0.1.7)
Criteria for variant exclusion	HapMap SNPs with average heterozygosity $\geq .02$ (dbSNP135), variants with MAF $>.0007$ in $>11,000$ internal exomes, or SNV quality <30
Read depth	
Mean	142x
$\geq 8x$	99.5 %
$\geq 20x$	98.4 %
Number of identified variants	
Putative bi-allelic	19
Putative <i>de novo</i>	Not available
Putative X-linked	4

7.2 *In silico* analysis results

Table S2: In silico analysis results (continued on following page)

Prediction tools:	Prediction for: c.336C>A (p.Ser112Arg)	Prediction tools:	Prediction for: c.339G>A
PROVEAN prediction (score)¹	Deleterious (-4.09)	TraP prediction (score)²	Benign (0.024)
SIFT prediction (score)³	Damaging (0)	DDIG prediction (raw score)⁴	Neutral (0.018)
PolyPhen-2 prediction (score)⁵	Probably damaging (0.998)	CADD prediction (PHRED-like-C-score)⁶	Likely benign (12.39)
CADD prediction (PHRED-like-C-score)⁶	Deleterious (23.7)	DANN prediction (score)⁷	Neutral (0.700)
LRT prediction (LRT_{new} score)⁸	Deleterious (1.00)	Fathmm-MLK prediction (coding score)⁹	Deleterious (0.697), (accuracy: 69 %)
SNAP2 prediction (score)¹⁰	Effect (60)	PredictSNP2 prediction (accuracy)¹¹	Neutral (96 %)

¹ PROVEAN [81] scores equal or below the preset threshold of -2.50 are considered “deleterious”.

² TraP [93] score ranges from 0 to 1. The threshold for “benign” variants is set to 0.459. Scores between 0.459 and 0.93 can be classified “possibly damaging”. Values above 0.93 are considered “damaging”.

³ SIFT [82] scores <0.05 are considered to affect protein function, meaning to be “damaging”.

⁴ DDIG [94] raw score ranges from 0 to 1. Raw scores close to 1 are likely “pathogenic” and raw scores close to 0 can be considered “neutral”.

⁵ PolyPhen-2 [83] score evaluates amino acid substitutions. Values close to 1 are most likely to be “damaging”.

⁶ CADD [84] PHRED-like-C-scores above 20 can be considered “deleterious”, however a distinct cut-off values do not exist and can be set somewhere between values of 10 and 20.

⁷ DANN [95] score ranges from 0 to 1. Score values close to 1 are most likely to be “deleterious”.

⁸ LRT [85] new score ranges from 0 to 1. Score values close to 1 a considered to be “deleterious”.

⁹ Fathmm-MLK [96] scores represent p-values ranging from 0 to 1. Scores above 0.5 are considered “deleterious” and below 0.5 “benign”.

¹⁰ SNAP2 [86] score ranges from -100 to +100. Low values are considered neutral, whereas high scores predict a strong effect of the variant.

¹¹ PredictSNP2 [97] suggests a certain prediction for the variant and reports the expected accuracy.

Prediction tools:	Prediction for: c.336C>A (p.Ser112Arg)	Prediction tools:	Prediction for: c.339G>A
MutationAssessor prediction (score)¹²	Medium (3.135)	PhD-SNPg prediction (score)¹³	Benign (0.036)
VEST3 score¹⁴	0.954	Mutation-Taster2 prediction (probability)¹⁵	Disease causing (0.999)
MutationTaster2 prediction (probability)¹⁵	Disease causing (0.999)		
PMut prediction (score)¹⁶	Pathological (0.68)		
GERP++ score¹⁷	4.3		
PhastCons100way score¹⁸	1.00		

Continued from previous page.

¹² MutationAssessor [87] scores predict the functional impact of variants: $\leq 0,8$ means “neutral”, between 0,8-1,9 “low”, 1,9-3,5 “medium” and $\geq 3,5$ “high” impact.

¹³ PhD-SNPg [98] score ranges from 0 to 1. Values above 0.5 are considered “pathogenic”, otherwise “benign”.

¹⁴ VEST3 [88] scores range from 0 to 1, with values close to 1 strongly suggesting a relevant functional effect.

¹⁵ MutationTaster2 [89] suggests a certain prediction for the variant and reports the corresponding probability of the prediction.

¹⁶ PMut [90] score ranges between 0 and 1. Scores from 0 to 0.5 are classified “neutral”, from 0.5 to 1 “pathological”.

¹⁷ GERP++ [91] RS score ranges from -12.36 to 6.18 and evaluates the evolutionary constraint of the examined position. The higher the score, the more conserved it is.

¹⁸ PhastCons100way score [92] score evaluates the conservation of a certain site on the DNA ranking the sites from 0 to 1. The higher the score, the more conserved it is.

7.3 Detailed information about clinical findings of *TOR1A*-related AMC cases

7.3.1 General information, pregnancy and birth history

Table S3: General information, pregnancy and birth history

Family	Family A		Family B		Family C
Ethnicity / Consanguinity	Kosovar / No		Kosovar / No		Spanish / No
<i>TOR1A</i> variants	p.Arg288* hmz.		p.Arg288* hmz.		c.-3G>T; p.Ser112Arg; c.339G>A
Individual / Sex / Age	A-II:1 / M / Deceased	A-II:2 / M / Deceased	B-II:1 / M / Deceased	B-II:2 / M / Deceased	C-II:1 / M / 8 y.
Abnormal findings during pregnancy / Age of discovery	Yes (polyhydramnios) / NR	Yes (polyhydramnios, retrognathia, fetal hypokinesia) / NR	Yes (reduced fetal movements) / 39 w. g.	Yes (polyhydramnios & reduced fetal movements) / 32 w. g. & 37 w. g.	No
Delivery	38 4/7 w. g., C section	38 2/7 w. g., C section	39 w. g., C section	38 w. g., C section	NR
Birth weight / length / head circumference	2,860 g / NR / 34.5 cm	3,800 g / 45 cm / 35.5 cm	3,080 g / NR / 35 cm	3,000 g / 47.5 cm / 35 cm	3,120 g / 45 cm / 35 cm
Neonatal respiratory distress (APGAR)	Yes (5/4/6)	Yes (NR)	Yes (7/8/3)	Yes (7/7/8)	No (NR)
Facial dysmorphism	NR	Retrognathia	High arched palate	High arched palate, micrognathia	High arched palate
Poor spontaneous movements	Yes	Yes	Yes	Yes	Yes
Multiple contractures	Yes (proximal & distal)	Yes (proximal & distal)	Yes (proximal & distal)	Yes (proximal & distal)	Yes (proximal & distal)
Hip dislocation	Yes (bilateral)	Yes (bilateral)	Yes	NR	Yes
Scoliosis	Yes	NR	NR	Yes	No
Hernia	Yes (inguinal, left)	Yes (inguinal, bilateral)	Yes (inguinal, bilateral)	Yes (inguinal, bilateral)	Yes (umbilical)

Hmz.: Homozygous; m: Month(s); M: Male; NR: Not reported; p.: percentile; w: Week(s); w. g.: Weeks of gestation; y: Year(s)

7.3.2 Disease course

Table S4: Disease course

Individual	A-II:1	A-II:2	B-II:1	B-II:2	C-II:1
Motor delay	NA	Yes (no head control)	NA	NA	Yes (all milestones)
Cognitive delay	Yes (no eye contact, no visual recognition)	Yes (no eye contact, no visual recognition)	Yes (no eye contact, no visual recognition)	Yes (no eye contact, no visual recognition)	Yes (understands simple questions, limited language at age 8 y.)
Failure to thrive	NR	NR	Yes	Yes	No
Respiratory distress / Hiccup-like breathing	Yes (apnea, bradycardia & desaturations) / Yes	Yes / Yes	Yes / NR	Yes / NR	No / No
Bulbar dysfunction	Yes (no swallowing, poor suck, no cough reflex)	Yes (poor swallowing)	Yes (poor suck, dysphagia)	Yes (poor suck, dysphagia)	Yes (tube feeding during 1 st w. of life; dysarthria)
Abnormal eye movements	NR	Yes (upgaze deviation, no spontaneous movements)	NR	NR	Yes (limited upgaze)
Muscle weakness	Yes	Yes	Yes	Yes	Yes
Increased muscle tone	Yes	Yes	NR	NR	Yes
Axial hyperextension	NR	NR	No	NR	Yes
Involuntary movements	NR	Yes (myocloni)	Yes (myoclonus-like, trembling movements)	Yes (myoclonus-like, trembling movements)	Yes (dystonia-like hand movements until age 7 m.)
Deep tendon reflexes	NR	NR	Brisk	NR	Brisk
Improvement of contractures	NA	NA	NA	NA	Yes
Age / Cause of death	4 w. / Respiratory failure	11 w. / Respiratory failure	4 w. / Respiratory failure	5 w. / Respiratory failure	Alive

m: Month(s); NA: Not applicable; NR: Not reported; w: Week(s); y: Year(s)

7.3.3 Further diagnostic studies

Table S5: Further diagnostic studies

Individual	A-II:1	A-II:2	B-II:1	B-II:2	C-II:1
Brain MRI	ND	Abnormal myelination of motor cortex, optic & corticospinal tracts	Wide subependymal spaces & occipital horns, delayed myelination of occipital subcortical white matter	ND	Normal
EEG	NR	Normal	Normal	Normal	Normal
Audiometry	Normal (newborn hearing screening)	Normal (newborn hearing screening)	NR	NR	Partial neurosensory deafness
EMG & nerve conduction studies	Axonal neuropathy or motor neuron disease	Normal, including RNS	Normal	NR	Normal
Muscle biopsy	ND	Normal	Normal	ND	ND
Serum CK	Normal	Normal	Normal	NR	NR

CK: Creatine kinase; EEG: Electroencephalography; EMG: Electromyography; MRI: Magnetic resonance imaging; ND: Not done; NR: Not reported; RNS: Repetitive nerve stimulation

7.4 Anti-TorsinA (D-M2A8) antibody

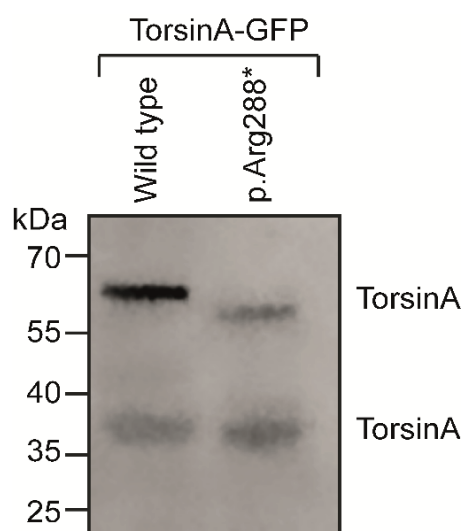


Figure S1: Anti-torsinA (D-M2A8) antibody

HEK293 cells were transiently transfected with wt- and p.Arg288*-*TOR1A*-GFP constructs. p.Arg288*-torsinA-GFP consist of the truncated aa-sequence of torsinA followed by the GFP tag. Anti-torsinA antibody was used to detect endogenous and overexpressed torsinA. The western blot shows that anti-torsinA antibody (D-M2A8) is suitable to detect the truncated aa sequence of p.Arg288* torsinA variant.

7.5 TorsinA expression in fibroblasts of AMC-cases

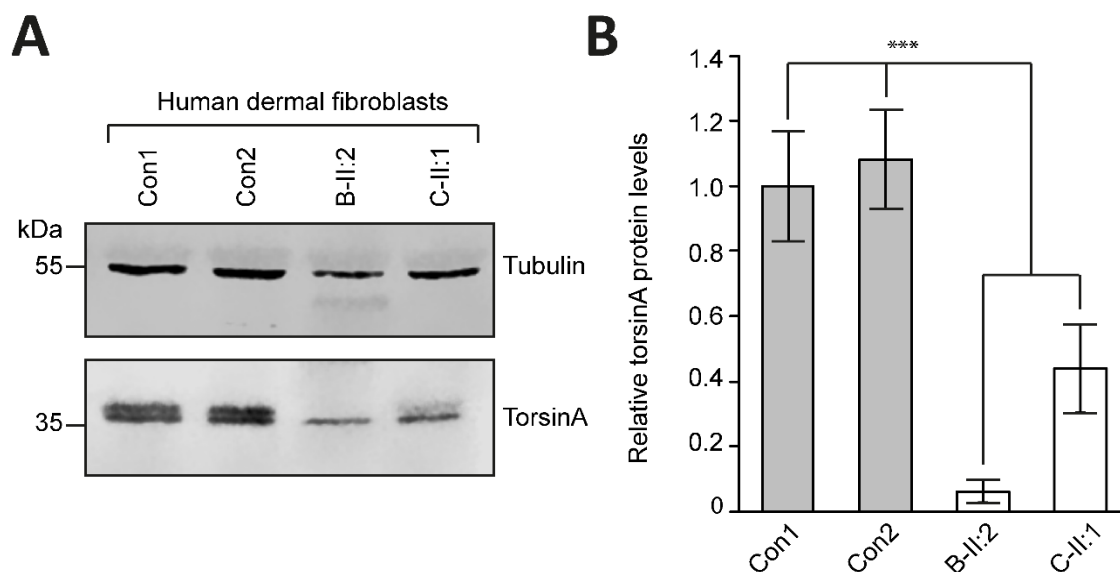


Figure S2: Endogenous torsinA levels in dermal fibroblasts of AMC-cases

(A) Representative western blot

Con1, Con2: control fibroblast cell lines; B-II:2, C-II:1: patients' fibroblasts. Protein lysates of patients' and control primary dermal fibroblasts were probed with anti-torsinA antibody (lower panel). TorsinA is assumed to run in the top of the double bands, the lower band is assumed to arise from unspecific antibody binding to human fibroblast proteins. α -tubulin (upper panel) was used as loading control.

(B) Quantification of endogenous torsinA levels

TorsinA levels were quantified and normalized to α -tubulin. Means and standard deviations of $n=3$ experiments are represented in the diagram. *** denotes $P<.001$, two-tailed Student's t-test.

7.6 Relative *TOR1A* mRNA levels in fibroblasts of AMC cases

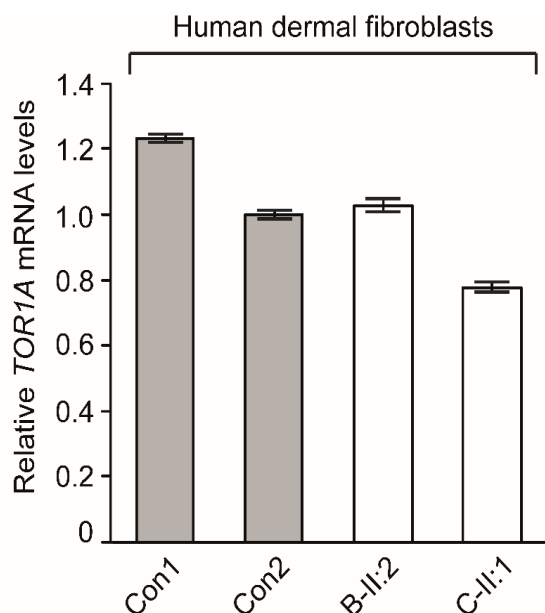


Figure S3: Relative *TOR1A* mRNA levels in dermal fibroblasts of AMC cases

Real-time qRT-PCR of *TOR1A* mRNA of primary human dermal fibroblasts. Con1, Con2: control cell lines; B-II:2, C-II:1: patients' fibroblasts. *TOR1A* mRNA signals were analyzed and normalized to *GAPDH* mRNA signals. Diagram represents mean values and standard deviations of n=3 experiments.

7.7 Online tools

7.7.1 *In silico* prediction tools

Ensembl Variant Effect Predictor (VEP) for GERP++, LRT, MutationAssessor, PROVEAN, SIFT, VEST3, PhastCons, PolyPhen-2, SNAP2 scores:

	https://www.ensembl.org/Tools/VEP
MutationTaster2:	http://www.mutationtaster.org/
PMut:	http://mmb.pcb.ub.es/PMut/analyses/new/
CADD:	https://cadd.gs.washington.edu/snv
FATHMM-MKL:	http://fathmm.biocompute.org.uk/fathmmMKL.htm
PhD-SNPg:	http://snps.biofold.org/phd-snpg/index.html
TraP:	http://trap-score.org/Search?version=v2
PredictSNP2:	https://loschmidt.chemi.muni.cz/predictsnp2/
DDIG:	http://sparks-lab.org/ddig/

7.7.2 Genome and exome databases

dbSNP:	https://www.ncbi.nlm.nih.gov/projects/SNP/
1000Genomes:	http://www.internationalgenome.org/
gnomAD:	https://gnomad.broadinstitute.org/
EVS:	http://evs.gs.washington.edu/EVS/

7.7.3 Tools for primer design and cloning

Primer3: <http://primer3.ut.ee/>
QuikChange
Primer Design: <https://www.agilent.com/store/primerDesignProgram.jsp>
NEBcutter V2.0: <http://nc2.neb.com/NEBcutter2/>

7.7.4 Other online tools

UniProt: <https://www.uniprot.org/uniprot/O14656>
Basic Local Alignment
Search Tool: <https://blast.ncbi.nlm.nih.gov/Blast.cgi>

8 Contributions

Physical examinations, history taking, apparative examinations and laboratory studies of the patients were performed or arranged by the following physicians: Jaume Colomer¹⁹, Sébastien Moutton²⁰, Claudine Rieubland²¹ and Johannes Lemke²². I reviewed and summarized the results for this study.

WES of patients A-II:1 and A-II:2 was performed by Tim M. Strom²³.

Pictures of patients A-II:1, A-II:2 and C-II:1 were taken by Claudine Rieubland and Jaume Colomer, who contributed them for this study.

RNA isolation and cDNA generation of *TORIA*, *TORIAIP1* and *TORIAIP2* was performed by Marina Dusl²⁴.

¹⁹ Unitat de Patologia Neuromuscular, Servei de Neurologia, Hospital Sant Joan de Déu, Barcelona, Spain

²⁰ Service de Génétique Médicale, CHU de Dijon, France

²¹ Division of Human Genetics, Department of Pediatrics, Inselspital, University of Bern, Switzerland

²² Institute of Human Genetics, University of Leipzig Hospitals and Clinics, Leipzig, Germany

²³ Institute of Human Genetics, Helmholtz Zentrum München, Neuherberg, Germany

²⁴ Friedrich-Baur-Institute at the Department of Neurology, University Hospital, LMU Munich, Munich, Germany

9 References

1. Oppenheim, H., *Über eine eigenartige Krampfkrankheit des kindlichen und jugendlichen Alters (dysbasia lordotica progressiva, dystonia musculorum deformans)*. Neurologie Centralblatt, 1911. **30**: p. 1090.
2. Fahn, S., *Concept and classification of dystonia*. Adv Neurol, 1988. **50**: p. 1-8.
3. Ozelius, L.J., et al., *The early-onset torsion dystonia gene (DYT1) encodes an ATP-binding protein*. Nat Genet, 1997. **17**(1): p. 40-8.
4. Bressman, S.B., et al., *Idiopathic dystonia among Ashkenazi Jews: evidence for autosomal dominant inheritance*. Ann Neurol, 1989. **26**(5): p. 612-20.
5. Park, J., et al., *Epidemiology of DYT1 dystonia: Estimating prevalence via genetic ascertainment*. Neurology. Genetics, 2019. **5**(5): p. e358-e358.
6. Bressman, S.B., et al., *Diagnostic criteria for dystonia in DYT1 families*. Neurology, 2002. **59**(11): p. 1780-2.
7. Bressman, S.B., et al., *The DYT1 phenotype and guidelines for diagnostic testing*. Neurology, 2000. **54**(9): p. 1746-52.
8. Albanese, A., et al., *Phenomenology and classification of dystonia: a consensus update*. Mov Disord, 2013. **28**(7): p. 863-73.
9. Ozelius, L. and N. Lubarr, *DYT1 Early-Onset Isolated Dystonia*, in *GeneReviews((R))*, M.P. Adam, et al., Editors. 1993, University of Washington, Seattle: Seattle (WA).
10. McNaught, K.S., et al., *Brainstem pathology in DYT1 primary torsion dystonia*. Ann Neurol, 2004. **56**(4): p. 540-7.
11. Paudel, R., et al., *Neuropathological features of genetically confirmed DYT1 dystonia: investigating disease-specific inclusions*. Acta Neuropathol Commun, 2014. **2**: p. 159.
12. Lumsden, D.E., et al., *Medication use in childhood dystonia*. Eur J Paediatr Neurol, 2016. **20**(4): p. 625-9.
13. Ozelius, L.J., N. Lubarr, and S.B. Bressman, *Milestones in dystonia*. Mov Disord, 2011. **26**(6): p. 1106-26.
14. Wichmann, T. and M.R. DeLong, *Deep Brain Stimulation for Movement Disorders of Basal Ganglia Origin: Restoring Function or Functionality?* Neurotherapeutics, 2016. **13**(2): p. 264-83.
15. Leung, J.C., et al., *Novel mutation in the TOR1A (DYT1) gene in atypical early onset dystonia and polymorphisms in dystonia and early onset parkinsonism*. Neurogenetics, 2001. **3**(3): p. 133-43.
16. Vulinovic, F., et al., *Unraveling cellular phenotypes of novel TorsinA/TOR1A mutations*. Hum Mutat, 2014. **35**(9): p. 1114-22.
17. Dobricic, V., et al., *Phenotype of non-c.907_909delGAG mutations in TOR1A: DYT1 dystonia revisited*. Parkinsonism Relat Disord, 2015. **21**(10): p. 1256-9.
18. Calakos, N., et al., *Functional evidence implicating a novel TOR1A mutation in idiopathic, late-onset focal dystonia*. J Med Genet, 2010. **47**(9): p. 646-50.

19. Zirn, B., et al., *Novel TOR1A mutation p.Arg288Gln in early-onset dystonia (DYT1)*. J Neurol Neurosurg Psychiatry, 2008. **79**(12): p. 1327-30.
20. Cheng, F.B., et al., *Combined occurrence of a novel TOR1A and a THAP1 mutation in primary dystonia*. Mov Disord, 2014. **29**(8): p. 1079-83.
21. Ritz, K., et al., *Myoclonus-dystonia: clinical and genetic evaluation of a large cohort*. J Neurol Neurosurg Psychiatry, 2009. **80**(6): p. 653-8.
22. Doheny, D., et al., *Clinical findings of a myoclonus-dystonia family with two distinct mutations*. Neurology, 2002. **59**(8): p. 1244-1246.
23. Cachecho, S., et al., *Arthrogryposis multiplex congenita definition: Update using an international consensus-based approach*. Am J Med Genet C Semin Med Genet, 2019. **181**(3): p. 280-287.
24. Hall, J.G., *Arthrogryposis multiplex congenita: etiology, genetics, classification, diagnostic approach, and general aspects*. J Pediatr Orthop B, 1997. **6**(3): p. 159-66.
25. Hall, J.G., *Arthrogryposis (multiple congenital contractures): diagnostic approach to etiology, classification, genetics, and general principles*. Eur J Med Genet, 2014. **57**(8): p. 464-72.
26. Staheli, L.T., et al., *Arthrogryposis: a text atlas*. 1998: Cambridge university press.
27. Reichert, S.C., P. Gonzalez-Alegre, and G.H. Scharer, *Biallelic TOR1A variants in an infant with severe arthrogryposis*. Neurol Genet, 2017. **3**(3): p. e154.
28. Isik, E., et al., *Biallelic TOR1A mutations cause severe arthrogryposis: A case requiring reverse phenotyping*. Eur J Med Genet, 2018.
29. Ozelius, L.J., et al., *The TOR1A (DYT1) gene family and its role in early onset torsion dystonia*. Genomics, 1999. **62**(3): p. 377-84.
30. Vander Heyden, A.B., et al., *Static retention of the luminal monotopic membrane protein torsinA in the endoplasmic reticulum*. Embo j, 2011. **30**(16): p. 3217-31.
31. Hewett, J., et al., *Mutant torsinA, responsible for early-onset torsion dystonia, forms membrane inclusions in cultured neural cells*. Hum Mol Genet, 2000. **9**(9): p. 1403-13.
32. Goodchild, R.E. and W.T. Dauer, *Mislocalization to the nuclear envelope: an effect of the dystonia-causing torsinA mutation*. Proc Natl Acad Sci U S A, 2004. **101**(3): p. 847-52.
33. Neuwald, A.F., et al., *AAA+: A class of chaperone-like ATPases associated with the assembly, operation, and disassembly of protein complexes*. Genome Res, 1999. **9**(1): p. 27-43.
34. Patel, S. and M. Latterich, *The AAA team: related ATPases with diverse functions*. Trends Cell Biol, 1998. **8**(2): p. 65-71.
35. Lupas, A., et al., *Self-compartmentalizing proteases*. Trends Biochem Sci, 1997. **22**(10): p. 399-404.
36. Walker, J.E., et al., *Distantly related sequences in the alpha- and beta-subunits of ATP synthase, myosin, kinases and other ATP-requiring enzymes and a common nucleotide binding fold*. Embo j, 1982. **1**(8): p. 945-51.

37. Babst, M., et al., *The Vps4p AAA ATPase regulates membrane association of a Vps protein complex required for normal endosome function*. *Embo j*, 1998. **17**(11): p. 2982-93.
38. Steel, G.J., et al., *A screen for dominant negative mutants of SEC18 reveals a role for the AAA protein consensus sequence in ATP hydrolysis*. *Mol Biol Cell*, 2000. **11**(4): p. 1345-56.
39. Zhu, L., et al., *A unique redox-sensing sensor II motif in TorsinA plays a critical role in nucleotide and partner binding*. *The Journal of biological chemistry*, 2010. **285**(48): p. 37271-37280.
40. Joshi, S.A., T.A. Baker, and R.T. Sauer, *C-terminal domain mutations in ClpX uncouple substrate binding from an engagement step required for unfolding*. *Mol Microbiol*, 2003. **48**(1): p. 67-76.
41. Hanson, P.I. and S.W. Whiteheart, *AAA+ proteins: have engine, will work*. *Nat Rev Mol Cell Biol*, 2005. **6**(7): p. 519-29.
42. DeLaBarre, B. and A.T. Brunger, *Complete structure of p97/valosin-containing protein reveals communication between nucleotide domains*. *Nat Struct Biol*, 2003. **10**(10): p. 856-63.
43. Goodchild, R.E. and W.T. Dauer, *The AAA+ protein torsinA interacts with a conserved domain present in LAPI and a novel ER protein*. *J Cell Biol*, 2005. **168**(6): p. 855-62.
44. Zhao, C., et al., *Regulation of Torsin ATPases by LAPI and LULL1*. *Proc Natl Acad Sci U S A*, 2013. **110**(17): p. E1545-54.
45. Ogura, T., S.W. Whiteheart, and A.J. Wilkinson, *Conserved arginine residues implicated in ATP hydrolysis, nucleotide-sensing, and inter-subunit interactions in AAA and AAA+ ATPases*. *J Struct Biol*, 2004. **146**(1-2): p. 106-12.
46. Sosa, B.A., et al., *How lamina-associated polypeptide 1 (LAPI) activates Torsin*. *Elife*, 2014. **3**: p. e03239.
47. Brown, R.S., et al., *The mechanism of Torsin ATPase activation*. *Proc Natl Acad Sci U S A*, 2014. **111**(45): p. E4822-31.
48. Rose, A.E., R.S. Brown, and C. Schlieker, *Torsins: not your typical AAA+ ATPases*. *Crit Rev Biochem Mol Biol*, 2015. **50**(6): p. 532-49.
49. Schmitt, J., et al., *Transmembrane protein Sun2 is involved in tethering mammalian meiotic telomeres to the nuclear envelope*. *Proceedings of the National Academy of Sciences*, 2007. **104**(18): p. 7426-7431.
50. Grady, R.M., et al., *Syne proteins anchor muscle nuclei at the neuromuscular junction*. *Proceedings of the National Academy of Sciences of the United States of America*, 2005. **102**(12): p. 4359-4364.
51. Zhang, X., et al., *Syne-1 and Syne-2 play crucial roles in myonuclear anchorage and motor neuron innervation*. *Development*, 2007. **134**(5): p. 901-8.
52. Crisp, M., et al., *Coupling of the nucleus and cytoplasm: Role of the LINC complex*. *The Journal of Cell Biology*, 2006. **172**(1): p. 41-53.
53. Starr, D.A. and J.A. Fischer, *KASH 'n Karry: the KASH domain family of cargo-specific cytoskeletal adaptor proteins*. *Bioessays*, 2005. **27**(11): p. 1136-46.

54. Wilhelmsen, K., et al., *KASH-domain proteins in nuclear migration, anchorage and other processes*. J Cell Sci, 2006. **119**(Pt 24): p. 5021-9.
55. Nery, F.C., et al., *TorsinA binds the KASH domain of nesprins and participates in linkage between nuclear envelope and cytoskeleton*. J Cell Sci, 2008. **121**(Pt 20): p. 3476-86.
56. Chang, L. and R.D. Goldman, *Intermediate filaments mediate cytoskeletal crosstalk*. Nat Rev Mol Cell Biol, 2004. **5**(8): p. 601-13.
57. Wilhelmsen, K., et al., *Nesprin-3, a novel outer nuclear membrane protein, associates with the cytoskeletal linker protein plectin*. J Cell Biol, 2005. **171**(5): p. 799-810.
58. Vander Heyden, A.B., et al., *LULL1 retargets TorsinA to the nuclear envelope revealing an activity that is impaired by the DYT1 dystonia mutation*. Mol Biol Cell, 2009. **20**(11): p. 2661-72.
59. VanGompel, M.J.W., et al., *A novel function for the Caenorhabditis elegans torsin OOC-5 in nucleoporin localization and nuclear import*. Molecular biology of the cell, 2015. **26**(9): p. 1752-1763.
60. Gomes, E.R., S. Jani, and G.G. Gundersen, *Nuclear movement regulated by Cdc42, MRCK, myosin, and actin flow establishes MTOC polarization in migrating cells*. Cell, 2005. **121**(3): p. 451-63.
61. Kupfer, A., D. Louvard, and S.J. Singer, *Polarization of the Golgi apparatus and the microtubule-organizing center in cultured fibroblasts at the edge of an experimental wound*. Proc Natl Acad Sci U S A, 1982. **79**(8): p. 2603-7.
62. Gundersen, G.G. and J.C. Bulinski, *Selective stabilization of microtubules oriented toward the direction of cell migration*. Proc Natl Acad Sci U S A, 1988. **85**(16): p. 5946-50.
63. Luxton, G.W., et al., *Linear arrays of nuclear envelope proteins harness retrograde actin flow for nuclear movement*. Science, 2010. **329**(5994): p. 956-9.
64. Saunders, C.A., et al., *TorsinA controls TAN line assembly and the retrograde flow of dorsal perinuclear actin cables during rearward nuclear movement*. J Cell Biol, 2017. **216**(3): p. 657-674.
65. Goodchild, R.E., C.E. Kim, and W.T. Dauer, *Loss of the dystonia-associated protein torsinA selectively disrupts the neuronal nuclear envelope*. Neuron, 2005. **48**(6): p. 923-32.
66. Jokhi, V., et al., *Torsin mediates primary envelopment of large ribonucleoprotein granules at the nuclear envelope*. Cell Rep, 2013. **3**(4): p. 988-95.
67. Pappas, S.S., et al., *TorsinA dysfunction causes persistent neuronal nuclear pore defects*. Hum Mol Genet, 2018. **27**(3): p. 407-420.
68. Burdette, A.J., et al., *The early-onset torsion dystonia-associated protein, torsinA, displays molecular chaperone activity in vitro*. Cell Stress Chaperones, 2010. **15**(5): p. 605-17.
69. Nery, F.C., et al., *TorsinA participates in endoplasmic reticulum-associated degradation*. Nat Commun, 2011. **2**: p. 393.

70. Chen, P., et al., *The early-onset torsion dystonia-associated protein, torsinA, is a homeostatic regulator of endoplasmic reticulum stress response*. Hum Mol Genet, 2010. **19**(18): p. 3502-15.
71. Pan, P.Y., J.H. Tian, and Z.H. Sheng, *Snapin facilitates the synchronization of synaptic vesicle fusion*. Neuron, 2009. **61**(3): p. 412-24.
72. Granata, A., et al., *The Dystonia-associated Protein TorsinA Modulates Synaptic Vesicle Recycling*. Journal of Biological Chemistry, 2008. **283**(12): p. 7568-7579.
73. Diril, M.K., et al., *Stonin 2 is an AP-2-dependent endocytic sorting adaptor for synaptotagmin internalization and recycling*. Dev Cell, 2006. **10**(2): p. 233-44.
74. Granata, A., et al., *CSN complex controls the stability of selected synaptic proteins via a torsinA-dependent process*. Embo j, 2011. **30**(1): p. 181-93.
75. Kakazu, Y., et al., *Synaptic vesicle recycling is enhanced by torsinA that harbors the DYT1 dystonia mutation*. Synapse, 2012. **66**(5): p. 453-464.
76. Shin, J.Y., et al., *Nuclear envelope-localized torsinA-LAP1 complex regulates hepatic VLDL secretion and steatosis*. J Clin Invest, 2019. **130**.
77. Grillet, M., et al., *Torsins Are Essential Regulators of Cellular Lipid Metabolism*. Dev Cell, 2016. **38**(3): p. 235-47.
78. Koressaar, T., et al., *Primer3_masker: integrating masking of template sequence with primer design software*. Bioinformatics, 2018. **34**(11): p. 1937-1938.
79. Koressaar, T. and M. Remm, *Enhancements and modifications of primer design program Primer3*. Bioinformatics, 2007. **23**(10): p. 1289-91.
80. Untergasser, A., et al., *Primer3--new capabilities and interfaces*. Nucleic acids research, 2012. **40**(15): p. e115-e115.
81. Choi, Y., et al., *Predicting the functional effect of amino acid substitutions and indels*. PLoS One, 2012. **7**(10): p. e46688.
82. Kumar, P., S. Henikoff, and P.C. Ng, *Predicting the effects of coding non-synonymous variants on protein function using the SIFT algorithm*. Nat Protoc, 2009. **4**(7): p. 1073-81.
83. Adzhubei, I.A., et al., *A method and server for predicting damaging missense mutations*. Nat Methods, 2010. **7**(4): p. 248-9.
84. Kircher, M., et al., *A general framework for estimating the relative pathogenicity of human genetic variants*. Nat Genet, 2014. **46**(3): p. 310-5.
85. Chun, S. and J.C. Fay, *Identification of deleterious mutations within three human genomes*. Genome Res, 2009. **19**(9): p. 1553-61.
86. Hecht, M., Y. Bromberg, and B. Rost, *Better prediction of functional effects for sequence variants*. BMC Genomics, 2015. **16**(8): p. S1.
87. Reva, B., Y. Antipin, and C. Sander, *Predicting the functional impact of protein mutations: application to cancer genomics*. Nucleic Acids Res, 2011. **39**(17): p. e118.
88. Carter, H., et al., *Identifying Mendelian disease genes with the variant effect scoring tool*. BMC Genomics, 2013. **14 Suppl 3**: p. S3.

89. Schwarz, J.M., et al., *MutationTaster evaluates disease-causing potential of sequence alterations*. Nat Methods, 2010. **7**(8): p. 575-6.
90. Lopez-Ferrando, V., et al., *PMut: a web-based tool for the annotation of pathological variants on proteins, 2017 update*. Nucleic Acids Res, 2017. **45**(W1): p. W222-w228.
91. Davydov, E.V., et al., *Identifying a high fraction of the human genome to be under selective constraint using GERP++*. PLoS Comput Biol, 2010. **6**(12): p. e1001025.
92. Pollard, K.S., et al., *Detection of nonneutral substitution rates on mammalian phylogenies*. Genome Res, 2010. **20**(1): p. 110-21.
93. Gelfman, S., et al., *Annotating pathogenic non-coding variants in genic regions*. Nat Commun, 2017. **8**(1): p. 236.
94. Livingstone, M., et al., *Investigating DNA-, RNA-, and protein-based features as a means to discriminate pathogenic synonymous variants*. Hum Mutat, 2017. **38**(10): p. 1336-1347.
95. Quang, D., Y. Chen, and X. Xie, *DANN: a deep learning approach for annotating the pathogenicity of genetic variants*. Bioinformatics, 2015. **31**(5): p. 761-3.
96. Shihab, H.A., et al., *An integrative approach to predicting the functional effects of non-coding and coding sequence variation*. Bioinformatics, 2015. **31**(10): p. 1536-43.
97. Bendl, J., et al., *PredictSNP2: A Unified Platform for Accurately Evaluating SNP Effects by Exploiting the Different Characteristics of Variants in Distinct Genomic Regions*. PLoS Comput Biol, 2016. **12**(5): p. e1004962.
98. Capriotti, E. and P. Fariselli, *PhD-SNPg: a webserver and lightweight tool for scoring single nucleotide variants*. Nucleic Acids Res, 2017. **45**(W1): p. W247-w252.
99. The Genomes Project, C., et al., *A global reference for human genetic variation*. Nature, 2015. **526**: p. 68.
100. Karczewski, K.J., et al., *Variation across 141,456 human exomes and genomes reveals the spectrum of loss-of-function intolerance across human protein-coding genes*. bioRxiv, 2019: p. 531210.
101. Ho, S.N., et al., *Site-directed mutagenesis by overlap extension using the polymerase chain reaction*. Gene, 1989. **77**(1): p. 51-9.
102. Livak, K.J. and T.D. Schmittgen, *Analysis of relative gene expression data using real-time quantitative PCR and the 2⁻(Delta Delta C(T)) Method*. Methods, 2001. **25**(4): p. 402-8.
103. Yu, P., et al., *FGF2 sustains NANOG and switches the outcome of BMP4-induced human embryonic stem cell differentiation*. Cell Stem Cell, 2011. **8**(3): p. 326-34.
104. Abdul Ghani, R., et al., *Ornithine decarboxylase gene expression in human lung adenocarcinoma cell (A549) treated with pomegranate juice*. Jurnal Teknologi, 2015. **77**.

105. Gomes, E.R. and G.G. Gundersen, *Real-time centrosome reorientation during fibroblast migration*. *Methods Enzymol*, 2006. **406**: p. 579-92.
106. Kariminejad, A., et al., *TOR1A variants cause a severe arthrogryposis with developmental delay, strabismus and tremor*. *Brain*, 2017. **140**(11): p. 2851-2859.
107. Thermann, R., et al., *Binary specification of nonsense codons by splicing and cytoplasmic translation*. *The EMBO journal*, 1998. **17**(12): p. 3484-3494.
108. Demircioglu, F.E., et al., *Structures of TorsinA and its disease-mutant complexed with an activator reveal the molecular basis for primary dystonia*. *Elife*, 2016. **5**.
109. Kozak, M., *An analysis of 5'-noncoding sequences from 699 vertebrate messenger RNAs*. *Nucleic Acids Res*, 1987. **15**(20): p. 8125-48.
110. Kozak, M., *Point mutations close to the AUG initiator codon affect the efficiency of translation of rat preproinsulin in vivo*. *Nature*, 1984. **308**(5956): p. 241-6.
111. Kozak, M., *Possible role of flanking nucleotides in recognition of the AUG initiator codon by eukaryotic ribosomes*. *Nucleic Acids Res*, 1981. **9**(20): p. 5233-52.
112. Desmet, F.O., et al., *Human Splicing Finder: an online bioinformatics tool to predict splicing signals*. *Nucleic Acids Res*, 2009. **37**(9): p. e67.
113. Obrig, T.G., et al., *The mechanism by which cycloheximide and related glutarimide antibiotics inhibit peptide synthesis on reticulocyte ribosomes*. *J Biol Chem*, 1971. **246**(1): p. 174-81.
114. Kerridge, D., *The effect of actidione and other antifungal agents on nucleic acid and protein synthesis in Saccharomyces carlsbergensis*. *J Gen Microbiol*, 1958. **19**(3): p. 497-506.
115. Giles, L.M., et al., *Dystonia-associated mutations cause premature degradation of torsinA protein and cell-type-specific mislocalization to the nuclear envelope*. *Hum Mol Genet*, 2008. **17**(17): p. 2712-22.
116. Gordon, K.L. and P. Gonzalez-Alegre, *Consequences of the DYT1 mutation on torsinA oligomerization and degradation*. *Neuroscience*, 2008. **157**(3): p. 588-95.
117. Kozak, M., *Point mutations define a sequence flanking the AUG initiator codon that modulates translation by eukaryotic ribosomes*. *Cell*, 1986. **44**(2): p. 283-92.
118. Naismith, T.V., S. Dalal, and P.I. Hanson, *Interaction of torsinA with its major binding partners is impaired by the dystonia-associated DeltaGAG deletion*. *J Biol Chem*, 2009. **284**(41): p. 27866-74.
119. Kock, N., et al., *Effects of genetic variations in the dystonia protein torsinA: identification of polymorphism at residue 216 as protein modifier*. *Hum Mol Genet*, 2006. **15**(8): p. 1355-64.
120. Dominguez Gonzalez, B., et al., *Excess LINC complexes impair brain morphogenesis in a mouse model of recessive TOR1A disease*. *Human Molecular Genetics*, 2018. **27**(12): p. 2154-2170.

121. Liang, C.-C., et al., *TorsinA hypofunction causes abnormal twisting movements and sensorimotor circuit neurodegeneration*. The Journal of clinical investigation, 2014. **124**(7): p. 3080-3092.
122. Jungwirth, M., et al., *Relative tissue expression of homologous torsinB correlates with the neuronal specific importance of DYT1 dystonia-associated torsinA*. Hum Mol Genet, 2010. **19**(5): p. 888-900.
123. Vasudevan, A., X.O. Breakefield, and P.G. Bhide, *Developmental patterns of torsinA and torsinB expression*. Brain research, 2006. **1073-1074**: p. 139-145.
124. Bahn, E., et al., *TorsinB expression in the developing human brain*. Brain Res, 2006. **1116**(1): p. 112-9.
125. Kim, C.E., et al., *A molecular mechanism underlying the neural-specific defect in torsinA mutant mice*. Proc Natl Acad Sci U S A, 2010. **107**(21): p. 9861-6.
126. Tanabe, L.M., C.C. Liang, and W.T. Dauer, *Neuronal Nuclear Membrane Budding Occurs during a Developmental Window Modulated by Torsin Paralogs*. Cell Rep, 2016. **16**(12): p. 3322-3333.
127. Li, J., et al., *TorsinB overexpression prevents abnormal twisting in DYT1 dystonia mouse models*. Elife, 2020. **9**.
128. Yokoi, F., et al., *Improved survival and overt "dystonic" symptoms in a torsinA hypofunction mouse model*. Behav Brain Res, 2020. **381**: p. 112451.
129. Duan, J., et al., *Synonymous mutations in the human dopamine receptor D2 (DRD2) affect mRNA stability and synthesis of the receptor*. Hum Mol Genet, 2003. **12**(3): p. 205-16.
130. Chamary, J.V., J.L. Parmley, and L.D. Hurst, *Hearing silence: non-neutral evolution at synonymous sites in mammals*. Nature Reviews Genetics, 2006. **7**(2): p. 98-108.
131. Sauna, Z.E. and C. Kimchi-Sarfaty, *Understanding the contribution of synonymous mutations to human disease*. Nature Reviews Genetics, 2011. **12**(10): p. 683-691.

10 Eidesstattliche Versicherung

Ich erkläre hiermit an Eides statt, dass ich die vorliegende Dissertation mit dem Titel

“Characterization of novel *TOR1A* variants causing extreme phenotypes of arthrogryposis multiplex congenita”

selbstständig verfasst, mich außer der angegebenen keiner weiteren Hilfsmittel bedient und alle Erkenntnisse, die aus dem Schrifttum ganz oder annähernd übernommen sind, als solche kenntlich gemacht und nach ihrer Herkunft unter Bezeichnung der Fundstelle einzeln nachgewiesen habe.

Ich erkläre des Weiteren, dass die hier vorgelegte Dissertation nicht in gleicher oder in ähnlicher Form bei einer anderen Stelle zur Erlangung eines akademischen Grades eingereicht wurde.

München, den 23.07.2023

Michael Thomas Pascher